Hazards of decreasing marine oxygen: the near-term and millennial-scale benefits of meeting the Paris climate targets

Gianna Battaglia[1,2] and Fortunat Joos[1,2]

[1]Climate and Environmental Physics, Physics Institute, University of Bern, Bern, Switzerland
[2]Oeschger Centre for Climate Change Research, University of Bern, Bern, Switzerland

Correspondence to: Gianna Battaglia (battaglia@climate.unibe.ch)

Abstract. Ocean deoxygenation is recognized as key ecosystem stressor of the future ocean and associated climate-related ocean risks are relevant for policy decisions today. In particular, benefits of reaching the ambitious 1.5 °C warming target mentioned by the Paris Agreement compared to higher temperature targets are of high interest. Here, we model oceanic oxygen, warming, and their compound hazard in terms of metabolic conditions on multi-millennial timescales for a range of temperature targets. Scenarios, where radiative forcing is stabilized by 2300, are used in ensemble simulations with the Bern3D Earth System Model of Intermediate Complexity. Transiently, the global mean ocean oxygen concentration decreases by a few percent under low and by 40 % under high forcing. Deoxygenation peaks about thousand years after stabilization of radiative forcing and new steady state conditions establish after AD 8000 in our model. Hypoxic waters expand over the next millennium and recovery is slow and remains incomplete under high forcing. Largest transient decreases in oxygen are projected for the deep sea. Distinct and close to linear relationships between the equilibrium temperature response and marine O_2 loss emerge. These point to the effectiveness of the Paris climate target in reducing marine hazards and risks. Mitigation measures are projected to reduce peak decreases in oceanic oxygen inventory by 4.4 % $°C^{-1}$ of avoided equilibrium warming. In the upper ocean, the decline of a metabolic index, quantified by the ratio of O_2 supply to an organism's O_2 demand, is reduced by 6.2 % $°C^{-1}$ of avoided equilibrium warming. Measures of peak hypoxia exhibit a strong sensitivity to additional warming. Volumes of water with less than 50 mmol O_2 m^{-3}, for instance, increase between 36 % to 76 % $°C^{-1}$ of equilibrium temperature response. Our results show that millennial-scale responses should be considered in assessments of ocean deoxygenation and associated climate-related ocean risks. Peak hazards occur long after stabilization of radiative forcing and new steady state conditions establish after AD 8000.

1 Introduction

Several key marine and coastal ecosystems are recognized to face high risk of impact due to climate change even if low emissions pathways are followed to the end of the century (*Gattuso et al.*, 2015; *Magnan et al.*, 2016). The most prominent marine ecosystem stressors include warming , acidification, deoxygenation, hypocapnia, changes in food supply and sea-level rise (*Gruber*, 2011; *Cocco et al.*, 2013; *Bopp et al.*, 2013; *Gattuso et al.*, 2015; *Sweetman et al.*, 2017). Risks arise both from changes in mean environmental conditions in response to climate change and potential changes in the frequency and severity of extreme events. This growing body of concern contributed to motivate the 21st Conference of the Parties (COP21) to reach the Paris Agreement with the goal of keeping the global mean atmospheric temperature rise by the end of Oxygen (O_2) is a sparingly soluble gas and its abundance in the ocean is decreasing under ongoing global warming (*IPCC*, 2013). Decreasing O_2 concentrations, warming and changes in other environmental parameters forced by anthropogenic greenhouse gas (GHG) emissions pose high risks for marine ecosystems (*Gattuso et al.*, 2015). The parties of the 21st century to well below United Nations Framework Convention on Climate Change (*UNFCCC*, accessed 6. February 2018) and of the Paris Agreement note 'the importance of ensuring the integrity of all ecosystems, including Oceans' (*UNFCCC*, accessed 11. October 2017) and 'the threats of irreversible damage' (*UNFCCC*, accessed 6. February 2018, Article 3). Marine changes are projected to evolve on multi-century and millennial time scales with peak impacts occurring potentially long after stabilization of atmospheric GHG concentrations and peak temperatures. Yet, only few studies assess millennial scale impacts of anthropogenic GHG emissions on the ocean and the reversibility of marine changes in oxygen. Explicit quantification of the benefits of meeting the 2°C, if not below 1.5 °C, above preindustrial (*Magnan et al.*, 2016; *UNFCCC*, accessed 11. October 2017). It is now a key scientific task to further assess what the impacts of global warming of C or 1.5 2 °C are on the ocean, not just by the end of the 21st century but on the typical equilibration timescale of the ocean which spans several millennia. Here we consider potential changes in oceanic oxygenand the hazard of hypoxia across a range of warming targets over the next 8000 years within the Bern3D Earth System Model of Intermediate Complexity (EMIC).

Oxygen (O_2) is a sparingly soluble gas and its distribution in the ocean results from the sum of its solubility component set trough air-sea exchange, the effect of O_2 production by phytoplankton in the euphotic zone and OC climate targets of the Paris Agreement with respect to the reversibility and avoidance of implied impacts on marine oxygen and related environmental parameters, including ocean circulation, ocean warming, metabolic viability and biological productivity is missing.

Typical thresholds leading to O_2consumption during organic matter remineralization at depth. Typical thresholds for hypoxia are approximately -stress for many macroorganisms (hypoxia) are around 50 mmol O_2 m^{-3}. Water with lower O_2 concentrations are effectively dead zones for many higher animals (reviewed in *Keeling et al.*, 2010; *Storch et al.*, 2014)(reviewed in *Keeling et al.*, 2 Species are also sensitive to thermal stress (*Gattuso et al.*, 2015) and their sensitivity to hypoxia increases with higher temperatures (*Pörtner*, 2010). In the modern ocean, oxygen-poor zones with $O_2 < 50$ mmol m^{-3} occupy about 5 % of its volume (*Garcia et al.*, 2014; *Bianchi et al.*, 2012). Expanding oxygen-poor waters lead to habitat compression, mortality and major

changes in community structure where energy preferentially flows into microbial pathways to the detriment of higher trophic levels. ~~Suboxia~~ Suboxic (<5 mmol O_2 m^{-3}) or anaerobic conditions can also lead to production of poisonous H_2S within sediments ~~(reviewed in *Diaz and Rosenberg*, 2008)~~(reviewed in *Diaz and Rosenberg*, 2008; *Breitburg et al.*, 2018) and decreasing O_2 concentrations potentially lead to higher production and emissions of the greenhouse gas nitrous oxide.

Observational (*Schmidtko et al.*, 2017; *Ito et al.*, 2017) and modeling studies (*Oschlies et al.*, 2017) indicate an overall decline in the oceanic oxygen content over past decades. Systematic discrepancies exist for the typically low oxygen tropical thermocline, where observations suggest O_2 has decreased and most models simulate increased O_2 levels over the past decades. Model projections to the end of the 21st century consistently project the global ocean oxygen inventory to further decline ~~(*Matear*, 2000; *Plattner et al.*, 2001; *Bopp et al.*, 2002; *Frölicher et al.*, 2009; *Cocco et al.*, 2013; *Bopp et al.*, 2013).~~ with anthropogenic climate change (*Matear*, 2000; *Plattner et al.*, 2001; *Bopp et al.*, 2002; *Frölicher et al.*, 2009; *Cocco et al.*, 2013; *Bopp et al.*, 2013). The most recent generation of Earth system models simulate global deoxygenation by the end of the 21st century of round -1.81% (RCP2.6) to -3.45% (RCP8.5) (*IPCC*, 2013). Impact studies have highlighted potential habitat compression (*Deutsch et al.*, 2015; *Mislan et al.*, 2017) and reduced catch potential (*Cheung et al.*, 2016) associated with climate change at the end of the century. Large model-model differences remain in projections of oxygen minimum zones (OMZs) (*Cocco et al.*, 2013; *Bopp et al.*, 2013).

~~The geologic record provides additional insight into sensitivities to climate change, even though the current increase in radiative forcing is more than an order of magnitude faster than any sustained change during the past 22, 000 years (*Joos and Spahni*, 2008). Oxygenation proxies reveal changes in oxygen for millennial scale processes and between glacial-interglacial transitions due to changes in ocean circulation and mixing, changes in oxygen consumption and solubility. For instance, atmospheric CO_2 and abyssal Southern Ocean oxygenation co-varied throughout the past 80~~

Given the long residence time of anthropogenic CO_2 in the atmosphere, and long equilibration timescales of the ocean overturning circulation, anthropogenic climate change will grow and persist beyond the end of the 21st century, the typical near-term assessment timescale of climate change (*Clark et al.*, 2016). Only few studies have assessed ocean biogeochemistry and the oceanic oxygen content beyond this near-term timescale. Available studies employ a range of physical and biogeochemical complexity levels from box models to general circulation models (GCMs). Oxygen concentrations are simulated to decline beyond the 21st century on multi-centennial timescales (*Matear and Hirst*, 2003; *Hofmann and Schellnhuber*, 2009; *Mathesius et al.*, 2015 Simulations covering two millennia show a recovery phase thereafter (*Schmittner et al.*, 2008; *Yamamoto et al.*, 2015). In most studies, simulated oxygen concentrations have not reached new steady state conditions at the end of the simulation. Low order Earth system models and Earth System Models of Intermediate complexity integrated by up to 100,000 years ~~reflecting enhanced deep ocean ventilation and less iron fertilization (*Jaccard et al.*, 2016). Also, abrupt warming events in the past have been shown to coincide with sudden appearance of hypoxia at intermediate depths in the North Pacific (*Praetorius et al.*, 2015) raising concern for impacts in the future. Across the last deglaciation, the deep ocean became better oxygenated and low oxygen water in the upper ocean expanded as the Earth transitioned to a warm interglacial state, opposite the general expectation from a pure~~

solubility point of view (*Jaccard and Galbraith*, 2012; *Jaccard et al.*, 2014). Earth System projections to have demonstrated the potential for long-term ocean oxygen depletion in response to carbon dioxide emissions and the long equilibration time scales of ocean biogeochemical variables in response to carbon emissions (*Shaffer et al.*, 2009; *Ridgwell and Schmidt*, 2010). Multi-millennial simulations are therefore required to assess the full amplitude of ocean biogeochemical changes and new steady state conditions due to anthropogenic climate change.

The distribution of O_2 in the ocean results from the sum of its solubility component set trough air-sea exchange, the effect of O_2 production by phytoplankton in the euphotic zone and O_2 consumption during organic matter remineralization at depth. In modeling studies, it is possible to identify the drivers of O_2 changes by considering changes due to solubility and changes due to oxygen consumption. When assessing the near-term timescale at the end of the 21st century are showing decreases in oxygen with warming and are therefore apparently in conflict with this geologic sense , studies have shown that different depths in the water column tend to be associated with different dominant mechanisms of change. Nevertheless, these simulations represent transient climate states and long term simulations are required for more adequate comparisons to past climate statesIn the surface ocean, O_2 changes tend to be determined by changes in O_2 solubility. In the subsurface, both changes in solubility and utilization may reinforce (mid and high latitudes) or compensate each other (tropics) (e.g. *Cabre et al.*, 2015; *Bopp et al.*, 2017). In the deep ocean, simulated O_2 changes are dominated by changes in O_2 utilization, which is in turn controlled by ocean ventilation (see also *Matear and Hirst*, 2003; *Yamamoto et al.*, 2015, for longer timescales). Changes in the oceanic heat content and in ocean circulation are therefore crucial for O_2 changes.

Deoxygenation is one of several marine ecosystem stressors including warming, acidification, hypocapnia, changes in food supply and sea-level rise (*Gruber*, 2011; *Cocco et al.*, 2013; *Bopp et al.*, 2013; *Gattuso et al.*, 2015; *Sweetman et al.*, 2017). Several key marine and coastal ecosystems may face high risk of impact due to climate change even if low emission pathways are followed to the end of the century (*Gattuso et al.*, 2015; *Magnan et al.*, 2016; *Breitburg et al.*, 2018). This growing body of concern contributed to motivate the 21st Conference of the Parties (COP21) to reach the Paris Agreement. Its goal is 'to strengthen the global response to the threat of climate change by keeping a global temperature rise this century well below 2 degrees Celsius above pre-industrial levels and to pursue efforts to limit the temperature increase even further to 1.5 degrees Celsius' (*UNFCCC*, accessed 11. October 2017). Well-defined metrics that summarize the Earth system response are useful in many aspects and may facilitate the communication in the mitigation policy context of the Paris agreement. The Transient Climate Response to Cumulative Carbon Emissions (TCRE, *Allen et al.*, 2009) or the Transient Earth System Response to Cumulative Carbon Emissions (TREX, *Steinacher and Joos*, 2016) are such metrics. These link changes in global surface air temperature and environmental parameters to cumulative CO_2 emissions relying on near linear relationships.

Here, we employ 4x100-member ensemble simulations with In this study, we assess the effectiveness of the Paris climate targets in reducing hazards of decreasing oceanic oxygen, ocean warming and marine export productivity as simulated by the Bern3D model Earth system model of intermediate complexity. To this end, we prescribe in the model four different scenarios where anthropogenic GHG forcing is stabilized by 2300 AD either under stringent mitigation limiting equilibrium global

surface air warming to 1.5 or 2°C above preindustrial or following business-as-usual 21th century emissions. Simulations are run to year AD 10,000 by which time the ocean has reached new steady state conditions. ~~Radiative forcing is prescribed to stabilize by 2300 and four different temperature targets are considered~~ This allows us assess reversibility and the full amplitude of changes, which are larger than the near-term changes at the end of the 21st century. We summarize the outcomes developing global metrics which quantify avoided marine hazards per avoided global warming.

In section 2, we briefly describe the Bern3D model and the experimental setup. Four different radiative forcing stabilization scenarios to meet four temperature targets (1.5, 1.9, 3.3 and 9.2°C above preindustrial) ~~. Each ensemble recognizes uncertainties in critical parameters of mixing and remineralization. We evaluate the response in oceanic oxygen content and a number of additional ecosystem stressors including warming , export production and~~ are considered. The observation-constrained 100-member ensembles used to explore parameter uncertainties for each scenario is introduced. In section 3, physical changes, including changes in overturning, water mass age, sea ice, temperature, salinity and density as well as biogeochemical changes, including changes in global oxygen inventory, the extent of oxygen minimum zones, and productivity are presented. The compound effects of warming and oxygen changes are assessed in the form of a metabolic index ~~. Oxygen changes arising from different contributions (production, consumption, solubility) are explicitly traced such that changes can be attributed to processes. We focus the description~~ (*Deutsch et al.*, 2015). Underlying physical and biogeochemical processes and mechanisms are discussed. Following earlier studies, we attribute the contributions of O_2 changes from changes in solubility, and the interplay of ocean biology and ventilation by carrying four explicit O_2 tracers and an ideal age tracer. The graphical illustration of spatial changes is focused on the 1.5 °C warming target ~~, the ambitious target~~ mentioned by the Paris Agreement~~. Avoided hazards compared to higher temperature targets are evaluated at the global scale. A range of multi-millennial projections available so far have focused primarily on the evolution of~~ , at the point of peak O_2 decline. Additional supporting figures are given in the appendix. In section 4, the relationship between change in global mean surface air temperature (~~SAT), atmospheric CO_2, oceanic pH, sea level and the Atlantic Meridional Overturning Circulation (AMOC)(*Plattner et al.*, 2008; *Eby et al.*, 2009; *Zickfeld et*~~

~~Fewer long-term model simulations have focused on oceanic oxygen (*Yamamoto et al.*, 2015; *Matear and Hirst*, 2003; *Schmittner et al.*, 20~~

~~We show that the oceanic oxygen equilibration timescale is considerably longer than its thermal equilibration timescale and that oceanic oxygen changes are dominated by changes in Atlantic and Indo-Pacific overturning, predictive variables to be considered in future multi-millennial projections with General Circulation Models (GCMs). We also highlight that a full account of climate-related ocean risks should include long-term, multi-millennial perspectives as most severe hazards occur long after stabilization of radiative forcing and the reduction of anthropogenic carbon emissions~~ΔSAT) and selected impact-relevant parameters is quantified. The different relationships are established for the near-term (2100 AD), the time of the peak decline in oxygen around 3000 to 4000 AD, and at year 10,000 AD when a new equilibrium has been reached in the model. Often relationships are near linear. This allows us to develop new metrics to quantify avoided marine hazards per unit change in ΔSAT. These quantitatively illustrate the benefits of meeting the Paris target in terms of marine hazards. Each modeling exercise is associated with uncertainties and in section 5, we discuss relevant uncertainties, mention neglected processes and

compare our findings to other studies. Finally, in section 6 we present implications and conclusions and summarize our findings graphically for a '1.5°C world' and contrast peak changes across the range of temperature targets.

2 Model and Simulations

2.1 Bern3D

The Bern3D Earth System Model of Intermediate Complexity is a three dimensional frictional geostrophic balance ocean model (*Müller et al.*, 2006), which includes a sea ice component coupled to a single-layer energy and moisture balance model of the atmosphere (*Ritz et al.*, 2011) and a prognostic marine biogeochemistry module (*Tschumi et al.*, 2011; *Parekh et al.*, 2008). A version with 41x40 horizontal grid-cells and 32 vertical layers is used (see also *Roth et al.*, 2014; *Battaglia et al.*, 2016 for model evaluation). The NCEP/NCAR monthly wind-stress climatology (*Kalnay et al.*, 1996) is prescribed at the surface. Air-sea gas exchange, carbonate chemistry and natural $\Delta^{14}C$ of DIC is modeled according to OCMIP-2 protocols (*Najjar et al.*, 1999; *Orr and Najjar*, 1999; *Orr and Epitalon*, 2015). The global mean air-sea transfer rate is reduced by 19 % compared to OCMIP-2 to match observation-based estimates of natural and bomb-produced radiocarbon (*Müller et al.*, 2008).

The biogeochemical module is based on phosphorus and simulates production and remineralization/dissolution of organic matter, calcium carbonate and opal. Production of particulate organic matter (POP) within the euphotic zone (top 75 m) depends on temperature, light availability, phosphate and iron following *Doney et al.* (2006). POP remineralization within the water column follows a power law profile (*Martin et al.*, 1987). Organic matter falling on to the sea floor is remineralized in the deepest box. Two thirds of organic matter production form dissolved organic matter (DOP), which decays with an e-folding lifetime of 1.5 years. An updated remineralization scheme assigns remineralization of POP and DOP to aerobic and anaerobic pathways depending on the mean grid-cell dissolved O_2 concentration (see ~~*Battaglia and Joos* (2017)~~*Battaglia and Joos* (2018)). We introduce two power law profiles with two distinct remineralization length scales for aerobic and anaerobic remineralization (α_{aerob} and α_{denit}). Constant stoichiometric ratios are used for both aerobic and anaerobic remineralization to convert biological P fluxes into carbon, and alkalinity fluxes (P:Alk:C=1:17:117). The O_2 demand for complete aerobic remineralization is 170 $\frac{molO_2}{molPO_4}$ and no oxygen is consumed for anaerobic remineralization. Accordingly, aerobic remineralization in the ocean is smaller than O_2 production in the euphotic zone leading to an O_2 outgassing for steady state conditions. The atmospheric oxygen inventory is constant. This is justified as 99.5 % of the ocean-atmosphere inventory is in the atmosphere and potential net fluxes of O_2 from the ocean and land to the atmosphere and fossil fuel burning have a small impact on atmospheric O_2. O_2 components from O_2 production, consumption and solubility are carried as explicit model tracers to attribute changes. Tracers add up to within 10^{-14} Pmol with mean inventories of 23.2, ~~-239.3, 429.9~~ -239, 430 yielding a total of ~~213.5~~ 214 Pmol, respectively (median values given). O_2 components inferred from O_2 saturation can result in systematic errors from surface disequilibrium (*Ito et al.*, 2004). The use of explicit tracers avoids such systematic errors in the O_2 components. As changes

in the O_2 production term are small, we combine the O_2 production and consumption tracers to a O_2 biology tracer when displaying sections.

We include evaluation of a metabolic index, Φ, which was proposed by *Deutsch et al.* (2015). It combines temperature and pO_2 as indicators of metabolically viable environments and is defined as the ratio of O_2 supply to an organism's resting O_2 demand. We consider only relative changes in $\Phi(t)$ relative to a reference time, t_0 (average over 1870-1899):.

$$\frac{\Delta\Phi(t)}{\Phi(t_0)} = \frac{pO_2(t)}{pO_2(t_0)} \times exp\left(\frac{E_0}{k_B}\left(\frac{1}{T(t)} - \frac{1}{T(t_0)}\right)\right) - 1, \quad (1)$$

where T is the absolute temperature, k_B is Boltzmann's constant and the exponential function and the parameter E_0 characterize the temperature dependence of the baseline metabolic rate. E_0 only weakly affects the relative influence of temperature and O_2 gradients and relative changes in Φ are therefore independent on species (*Deutsch et al.*, 2015). Here, we consider E_0=0.87 eV (representative of Atlantic cod). For the calculation of pO_2 we pressure-correct the equilibrium constant following Eq. 5 in *Weiss* (1974). The metabolic index Φ, as proposed by *Deutsch et al.* (2015), is linear in pO_2 (representing the rate of O_2 supply) and decreases non-linearly with temperature (indicative of the resting metabolic demand). One may note that the exponential curve varies approximately linearly for typical global warming associated temperature changes as $E_0/k_b (\approx$ 10,000 K) is large.

The current set up does not include sediment interactions, temperature dependent remineralization, variable stoichiometry, nitrogen-cycle feedbacks, atmospheric nutrient deposition, dynamic wind nor freshwater input/albedo changes from melting of continental ice-sheets.

2.2 Ensemble and scenarios

To explore potential oxygen changes we set up four 100-member ensembles each targeting a different equilibrium temperature response ($\sim$1.5, 1.9, 3.3 and 9.2 °C above preindustrial). A feedback parameter λ [W m^{-2} K^{-1}] (*Ritz et al.*, 2011), accounting for climate feedbacks that are not explicitly treated in the Bern3D model, is chosen in combination with radiative forcing from the Representative Concentration Pathways (RCPs) (*Meinshausen et al.*, 2011) to achieve these stabilization targets. RCP2.6, stabilizing by 2300, is run with λ values of -0.71 and -1 W m^{-2} K^{-1} achieving the 1.5 and 1.9 °C targets, respectively. RCP4.5, stabilizing after 2100, is run with -1 W m^{-2} K^{-1} yielding a 3.3 °C temperature response and RCP8.5, stabilizing in the 23rd century, with -0.71 W m^{-2} K^{-1} yielding a 9.2 °C response (median values given for temperature targets). Each member is spun up over 5000 years to AD 1765 boundary conditions. The radiative forcing follows RCP scenarios (RCP2.6, 4.5 and 8.5, *Meinshausen et al.*, 2011). The RCP scenarios are extended to year AD 10,000 by which time the ocean has equilibrated to new steady state conditions. Radiative forcing includes an 11-year solar cycle up to year AD 3000. After that, all forcings

are kept constant. We employ a single-model setup, and assess uncertainties arising from organic matter remineralization (α_{aerob} and α_{denit}) and vertical mixing ($k_{diff-dia}$). The three parameters are sampled using the Latin Hypercube sampling technique (*McKay et al.*, 1979). The parameter ranges are chosen such that all members achieve similar skill scores with respect to observation-derived fields of natural radiocarbon (*Key et al.*, 2004) and dissolved O_2 (*Garcia et al.*, 2014; *Bianchi et al.*, 2012) and correspond to the values chosen in ~~*Battaglia and Joos* (2017).~~ *Battaglia and Joos* (2018, Table 1). A normal distribution is used to sample α_{aerob} with a standard value of -0.83 and a standard deviation of -0.0625. α_{denit} is sampled uniformly between -0.1 and -0.01. And a lognormal distribution is used to sample $k_{diff-dia}$ (standard value=2.25E-5 $m^2\ s^{-1}$, shape parameter=0.2, location parameter=0). We choose a single ensemble member with parameter values close to the standard values as representative ensemble member to illustrate spatial anomalies (α_{aerob}=-0.85, α_{denit}=-0.037, $k_{diff-dia}$=2.05E-05 $m^2\ s^{-1}$).

2.3 Pre-Industrial characteristics

The ensemble produces a range in overturning strengths, remineralization fluxes and O_2 distributions. The following numbers represent the 90 % confidence ranges of important model characteristics across the ensemble. The ~~AMOC~~ maximum of the Atlantic meridional overturning streamfunction below 400 m depth (AMOC) ranges from 16.5 to 19.7 Sv~~,~~. The minimum of the Indo-Pacific meridional overturning streamfunction below 400 m depth (Indo-Pacific MOC) ranges between -13.6 to -15.6 Sv~~and export~~. Export of particulate organic matter at 75 m ranges from 9.0 to 11.4 Gt C yr^{-1}. The simulated oxygen inventory ranges between 195 and 230 Pmol given the three parameters and the simulated oxygen distribution covers the observational range ~~well (Fig. 7a in *Battaglia and Joos*, 2017)~~and spatial pattern well (see Fig. 3, Fig. 7a, Table D1 of *Battaglia and Joos*, 2018). Biases exist in the simulated extend of OMZs. The volume of suboxic conditions ($O_2 < 5$ mmol m^{-3}) is overestimated by a factor of five but water column denitrification fluxes are well within current estimates ~~(Table C.1., Fig. 2c in *Battaglia and Joos*, 2017)~~(Table D
This is a common model bias in EMICs and ~~GCMS~~ GCMs (*Cocco et al.*, 2013; *Bopp et al.*, 2013; *Cabre et al.*, 2015). Vastly enhanced spatial resolution may be required to simulate equatorial physics and ecosystems in better agreement with observations (*Bopp et al.*, 2013).

3 ~~Peak oxygen decreases scale linearly with forcing~~Marine changes in temperature, circulation and biogeochemistry

We first ~~explore how oxygen changes scale with forcing at different timescales (Fig. 4 and 2).~~ describe the evolution of important physical quantities that impact O_2 concentrations. Figure 1 displays the temporal changes in global mean surface air and ocean temperature, the evolution of sea-icea area in the Northern and Southern Hemisphere, and the Atlantic and Indo-Pacific meridional overturning circulation.

In response to the RCP scenarios, atmospheric temperatures rise and stabilize after ~1000 years (Fig. ~~2~~1a). The four ensembles reaching 1.5, 1.9, 3.3 and 9.2 °C above preindustrial surface air temperature show an equilibrium ocean warming of 1.1, 1.3, 2.0 and 5.5 °C, respectively (median values given). Sea ice retreats in both hemispheres (Fig. 1c,d). The retreat is more pronounced for higher forcing. In the Southern Hemisphere, even the lower forcing levels show strong decline in the sea-ice area and sea ice vanishes for higher forcing. The warming perturbation causes the AMOC and Indo-Pacific MOC to decline transiently (Fig. 1e,f, Fig. A1). The larger the forcing and implied changes in stratification, the larger the peak decline in overturning (Fig. 1e,f). The decline is likely driven by upper ocean warming, leading to increasing surface-to-deep density gradients as further modulated by salinity changes (Fig. A2). The deep ocean water mass age increases in response to the slowed overturning (Fig. 2d, 3d). As retreating sea-ice increases wind stress over these newly exposed areas, younger water masses form in the upper ocean of the Southern Ocean (Fig. 3d). As the model tends to equilibrate under the sustained radiative forcing, the surface-to-deep gradients in the density anomalies diminish (Fig. A2), the meridional overturning circulation recovers (Fig. 1e,f), and anomalies in water mass age become again smaller (Fig. 3d versus Fig. A3). The final circulation state is close to but not identical to the preindustrial steady state circulation. Maximum overturning strength in AMOC and the Indo-Pacific MOC varies by less than $\pm$ 1 Sv around the initial value. At the new steady state, the maximum in AMOC below 400 m tends to be lower under higher forcing, whereas the maximum in the Indo-Pacific MOC below 400 m tend to be higher under higher forcing (Fig. 1e,f). It is difficult and beyond the scope of this paper to conclusively explain such subtle changes in ocean dynamics and overturning (Fig. A1), likely linked to the complex changes in density (Fig. A2) and sea ice retreat (Fig. 1c,d). Yet, these differences have direct consequences for the projected global water mass age and by that for oceanic oxygen (Fig. 2) at the new equilibrium as further discussed below.

The response in oceanic oxygen is ~~more~~ complex and characterized by an initial decline followed by a recovery phase (Fig. 2~~b). Our~~ a). In line with earlier studies (*Matear and Hirst*, 2003; *Schmittner et al.*, 2008; *Shaffer et al.*, 2009; *Ridgwell and Schmidt*, 2 our results demonstrate the potential for large changes in marine oxygen under anthropogenic forcing, a large inertia in the response and a slow, and partially incomplete recovery of the perturbation. Transiently, the whole ocean oxygen inventory decreases by a few percent (6 %) under low forcing and by as much as 40 % under high forcing (median values given). The minimum in oxygen occurs about thousand years after stabilization of radiative forcing, and it takes several millennia to approach a new equilibrium. Then, the global ocean O_2 inventory is a few percent higher than at preindustrial conditions under low and intermediate forcing and remains depleted by around 8 % in the high forcing case.

~~The magnitude of changes in~~ Figure 2 further explains the temporal evolution and interplay of the underlying drivers. In all cases, the changes in global oxygen inventory (Fig. 2a) strongly correlate with water mass age (Fig. 2d) and are also impacted by gradual oxygen loss due to warming as evidenced by the evolution of the O_2 solubility tracer (Fig. 2b). Inventory changes based on the O_2 production tracer (Fig. 2c) are negligible; changes equilibrate with the atmosphere and only a small fraction remains in the ocean. The O_2 consumption tracer (Fig. 2e) determines the shape of the global O_2 signal (Fig. 2a). It correlates strongly with ideal age (Fig. 2d) and integrates changes in overturning and remineralization fluxes. Changes from remineralization fluxes include both changes in absolute aerobic remineralization fluxes and changes in the relative share of denitrification (Fig. 2i). An increased share of denitrification at organic matter remineralization, for instance, effectively constitutes an implicit O_2 gain. Denitrification fluxes correlate with the volumetric expansion of OMZs and are also impacted by changes in remineralization fluxes within them (Fig. 2i). The recovery level of the O_2 consumption tracer (Fig. 2e) reflects the global recovery level of ideal age (Fig. 2d), where younger water masses are associated with less O_2 consumption and therefore higher O_2 concentrations. The total O_2 recovery level (Fig. 2a), on the other hand, is diminished due to O_2 loss from solubility (Fig. 2b). As such, 1.5 to 3.3 °C warming targets reach similar global O_2 equilibrium levels for different reasons. The 1.9 and ~~related hazards generally increase with the magnitude of forcing and warming. Distinct and close to linear relationships~~ 3.3 °C warming targets tend to result in younger water masses, which would increase O_2 due to less O_2 consumption compared to 1.5 °C warming targets. As those scenarios are also associated with higher warming, they lose more O_2 due to less solubility compared to 1.5 °C warming targets and yield similar global anomalies despite more pronounced spatial patterns. The 9.2 °C warming target reaches a lower equilibrium O_2 inventory compared to preindustrial due to high O_2 loss from solubility (-44.1 Pmol).

We illustrate spatial changes in critical variables for a single, representative ensemble member (see Section 2.2) at its peak O_2 decline which occurs at year AD 3150 and amounts to 5 % (Fig. 3). The member eventually reaches a 1.5 °C warming target. Figure 3 displays anomalies in total O_2 (Fig. 3a), and the contributions from biologically-mediated changes (termed "biology" below, Fig. 3b) combining the changes in the O_2 production and consumption tracer and from changes in solubility (Fig. 3c). In the upper ocean O_2 concentrations tend to increase due to biology and decrease due to solubility. Such compensating mechanisms have been documented elsewhere (e.g. *Cabre et al.*, 2015; *Bopp et al.*, 2017). The resulting changes in O_2 are less pronounced than the changes in each component. The increase in O_2 due to biology stems from younger water masses and less export in the low- and mid latitudes (see next paragraph and Fig. 4c). O_2 changes show strong spatial correlation with changes in water mass age (Fig. 3a,d). Largest decreases in O_2 are simulated in bottom waters in line with older water mass age. The equilibrium response in O_2 for this 1.5 °C warming case is characterized by slight O_2 decreases in the Atlantic, caused mainly by less solubility, and increases in the Southern Ocean and deep Pacific, caused by higher overturning and less sea-ice coverage in the Southern Ocean compared to preindustrial (Fig. A3).

Global export production is simulated to decline over the first few centuries, and reach higher values under new steady state conditions (Fig. 2g). The decline is stronger for higher forcing, while the recovery level of global export production is

similar across the scenarios. Bern3D transiently simulates decreased export in the mid- and low latitudes (Fig. 4c, see also *Steinacher et al.* (2009); *Battaglia and Joos* (2018)) as a result of increased stratification (Fig. A2c,f,i) and reduced nutrient concentrations in the surface ocean (Fig. 4b). In the high latitudes, the model simulates increased export production, as a result of less temperature and light limitation as surface waters warm and sea ice retreats. This pattern of decreased export in mid- and low latitudes and increased export in high latitudes is similar across the scenarios. Export production in the low latitudes fully recovers for lower forcing and partially recovers for higher forcing. The lower recovery level in the low latitudes is compensated by higher increases in the high latitudes for high forcing. The magnitude of positive and negative changes increases with forcing, but the global anomalies remain comparable at the end of the simulation.

Next to changes in export, we consider the evolution of a metabolic index in the upper ocean which integrates effects of changes in O_2 and temperature at the organism level (Fig. 2f and Fig. 4e). The globally averaged, upper ocean (depth < 400 m) metabolic index declines throughout the simulation dominated by increased temperatures (Fig. 2f). The metabolic index, Φ (*Deutsch et al.*, 2015), decreases in most places in line with warming and lower pO_2 (Fig. 4a,d,e). The O_2 gain in upper ocean waters is able to counteract the adverse effect of warming in some high latitude environments. In other places with higher pO_2, the temperature increase dominates the response in Φ. Near bottom waters in the Pacific are prone to largest reductions in Φ, driven by large decreases in pO_2 (Fig. 4e).

Oxygen-poor waters (O_2 < 50 mmol m^{-3}, Fig. 2h) are simulated to transiently increase across all scenarios. The response is characterized by high uncertainty as introduced by the sampled parameters. Under new equilibrium conditions, the volume of low O_2 waters is reduced for low and intermediate forcing and remains higher than pre-industrial in the high forcing case.

Turning to uncertainties in our perturbed parameter ensemble, we find that variations in the vertical diffusion parameter ($k_{diff-dia}$) dominate the uncertainty in the globally-averaged evolution of ideal age, sea ice cover, temperature and O_2. The modeled uncertainty in the volume of low O_2 waters is dominated by different values of the α_{aerob} parameter. Whether a threshold in O_2 concentration is met depends on the pre-industrial tracer distribution. Longer remineralization length scales bring more remineralization to depth, leading to higher O_2 consumption.

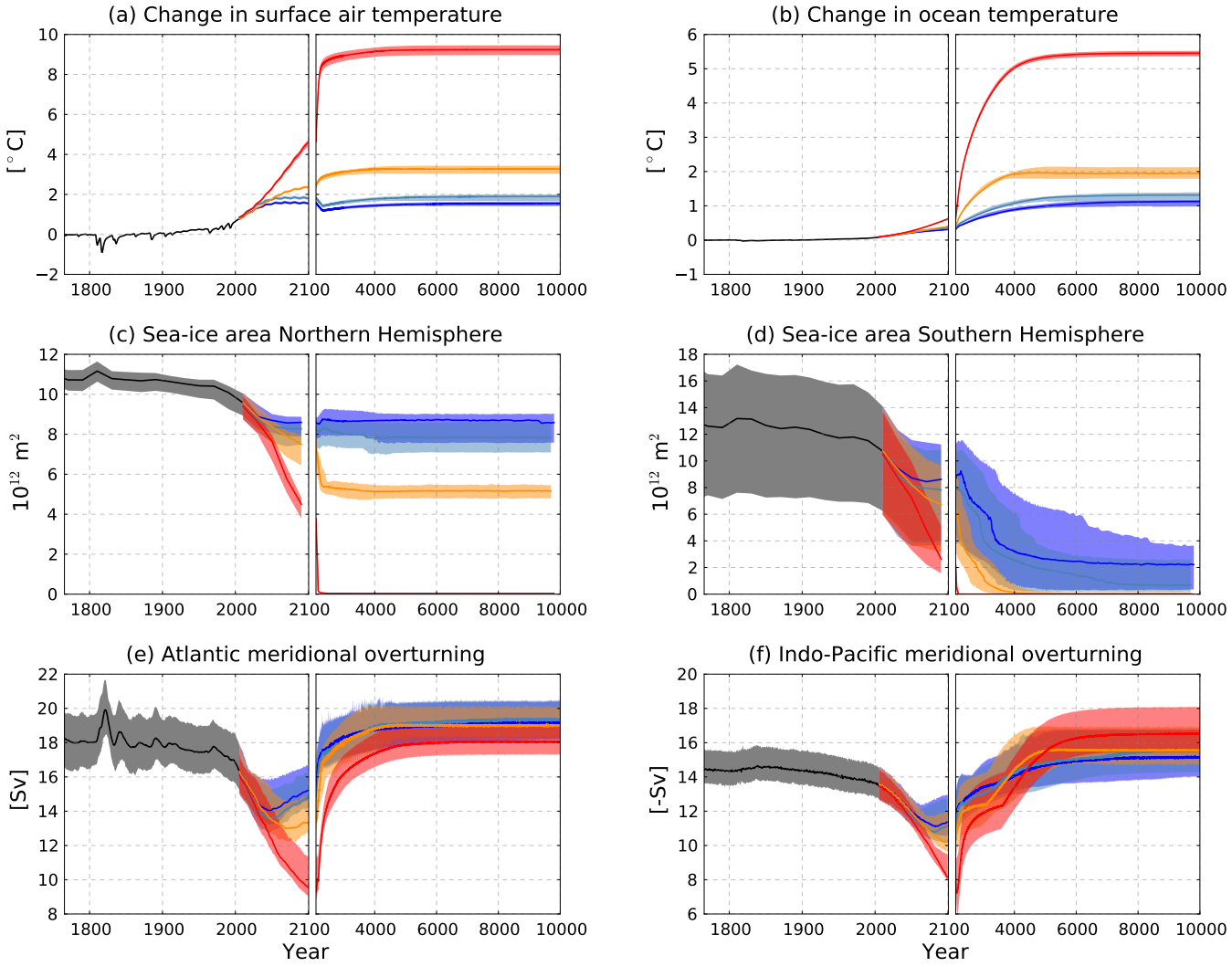

Figure 1. Temporal evolution of physical variables relative to 1870-1899 for model ensembles aiming at 1.5, 1.9, 3.3 and 9.2 °C warming targets. Lines mark the median and shading marks the 90 % range of the ensemble. The shading reflects uncertainties due to variations in the diapycnal mixing coefficient. e) Atlantic meridional overturning is the maximum of the Atlantic and f) Indo-Pacific meridional overturning is the minimum of the Indo-Pacific meridional overturning streamfunction below 400 m depth.

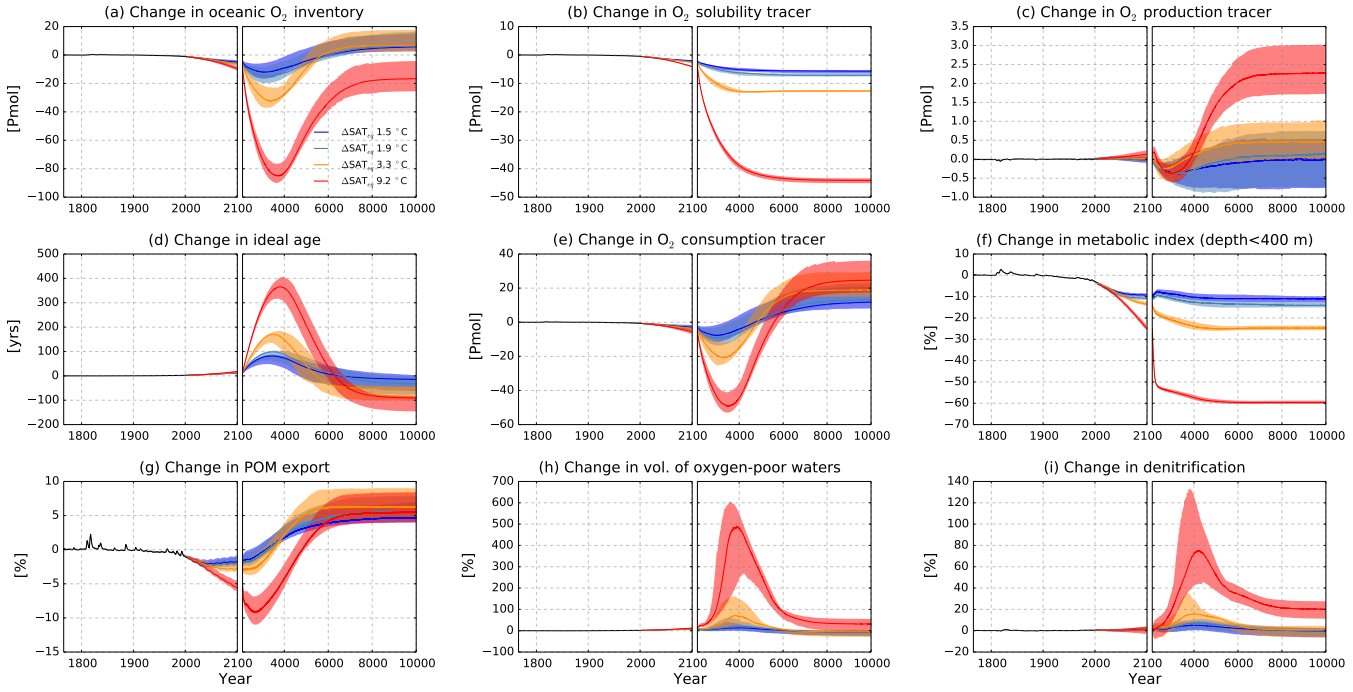

Figure 2. Temporal evolution of critical variables relative to 1870-1899 for model ensembles aiming at 1.5, 1.9, 3.3 and 9.2 °C warming targets. Lines mark the median and shading marks the 90 % range of the ensemble. The shading reflects uncertainties due to variations in the diapycnal mixing coefficient, and the aerobic and anaerobic remineralization length scales of particulate organic matter (α_{aerob} and α_{denit}). b) O_2 solubility is the explicitly traced solubility component of oceanic oxygen, c) is the explicit O_2 production tracer, e) is the explicit O_2 consumption tracer. h) Oxygen-poor waters are taken as the volume of water with $O_2 < 50$ mmol m^{-3}.

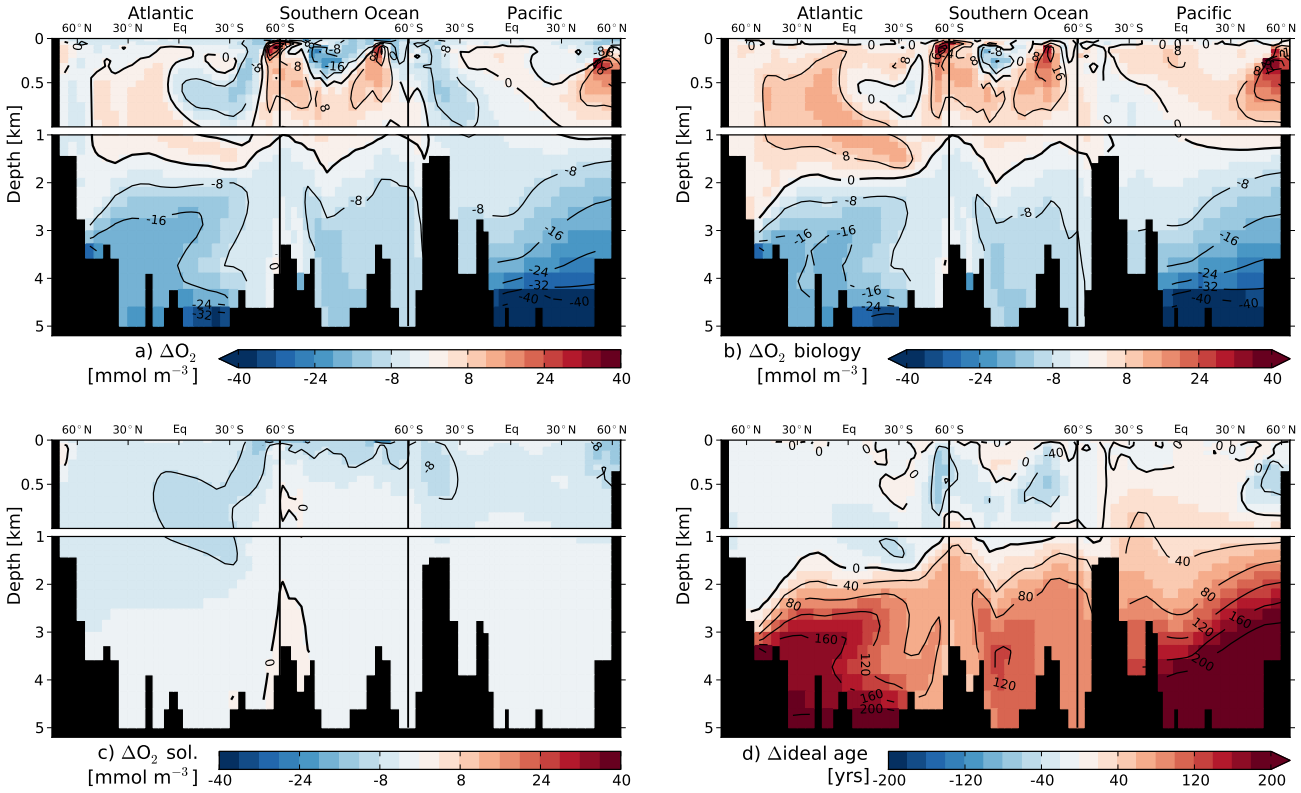

Figure 3. Changes in O_2 and its components at time of peak O_2 decline (AD 3150) relative to preindustrial steady state for a single, representative ensemble member reaching a 1.5 °C warming target. a) Change in total O_2, b) change in O_2 due to biology, c) change in O_2 due to solubility, d) change in ideal age.

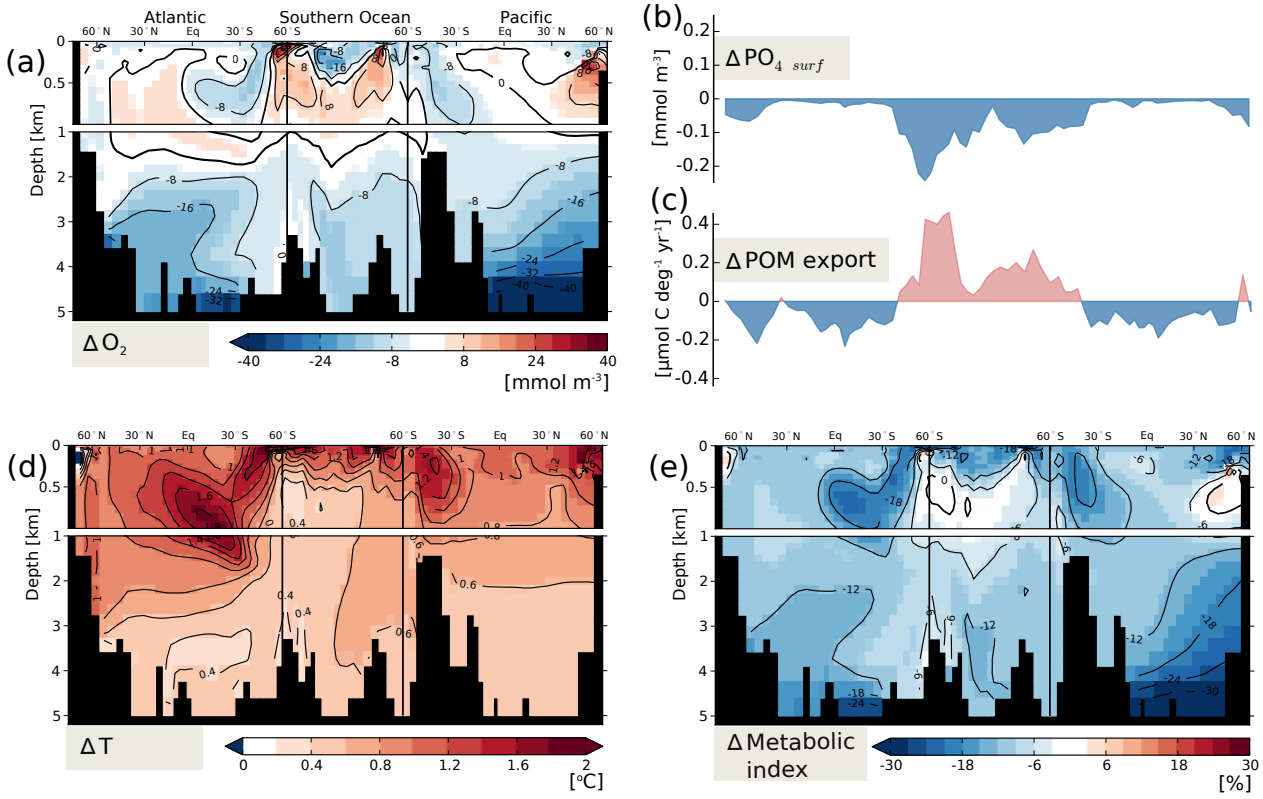

Figure 4. Changes in potential ecosystem stressors at peak O_2 decline (AD 3150) relative to preindustrial steady state for a single, representative ensemble member reaching a 1.5 °C warming target. Results are displayed for a cross section through the Atlantic (25° W), across the Southern Ocean (58° S) and into the Pacific (175° W). Changes in POM export at 75 m (c) and in surface PO_4 concentrations (d) are displayed along the same section.

4 Metrics linking global warming to marine hazards

The purpose of this section is to quantify the relationship between changes in ~~SAT and in~~ global mean surface air temperature (SAT), the target variable of the Paris Agreement, with selected aggregated metrics for marine ecosystem stressors. In this way, we link marine hazards to the temperature target of the Paris Agreement and quantify avoided marine change per unit of avoided global warming. Specifically, we investigate the relationship of SAT with changes in the marine O_2 ~~emerge.~~ inventory, ocean temperature, and the metabolic index of *Deutsch et al.* (2015), the volume occupied by hypoxic water and in low latitude export production (30°S - 30°N) across the range of warming scenarios in our ensemble (Fig. 4). Distinct and often close to linear relationships emerge. Near-linearity allows us to characterize the benefits of avoided warming by single sensitivities, corresponding to the slopes of the relationships displayed in Fig. 4.

The relationships between SAT and marine hazard metrics critically depend on the time horizon considered (Fig. 4). Larger magnitudes are simulated on millennial timescales compared to the near-term end of the 21st century. Assessment of ocean deoxygenation by the end of the 21st century, therefore, underestimates the full amplitude of change.

Transient (end of 21st century), peak (AD ∼3000) and equilibrium (AD ∼8000) oxygen changes exhibit distinct relationships to their corresponding warming (Fig. 4a). At the end of the 21st century, simulated oxygen decreases by 0.68 % $°C^{-1}$ of realized warming (median values). At peak oxygen decline, this sensitivity increases and oxygen decreases by 4.4 % $°C^{-1}$ of equilibrium temperature response. In other words, an avoided warming of 1°C, avoids a peak decline in marine O_2 inventory of 4.4%. The linear relationship breaks down for the equilibrium response. While 1.5 to 3.3 °C warming targets lead to similar and higher oxygen levels, the 9.2 °C warming target results in lower oxygen levels compared to preindustrial ~~. The sensitivities across different timescales are very similar across the~~ as discussed in the previous section. The relationships generally hold across the sampled parameter space. ~~Lower mixing coefficients lead to larger decreases in absolute terms.~~

The volume of low oxygen waters is particularly sensitive to warming and parameter uncertainty (Fig. 4b). We illustrate the sensitivities at the example of the volume of waters with $O_2 < 50$ mmol m^{-3}. At the end of the 21st century, there is a 1.7 % increase in this volume per °C of realized warming. Peak increases scale with 63 % $°C^{-1}$ of equilibrium temperature response. Uncertainties in remineralization cause a spread in this response ranging from 36-76 % $°C^{-1}$ of equilibrium temperature response (90 % confidence range): The ~~deeper~~ longer the remineralization length scale, the higher this sensitivity. Pre-existing low O_2 waters expand and new low O_2 waters may develop in near bottom environments for higher forcing levels. While the lower temperature targets yield lower volumes of low oxygen waters, the 9.2 °C target yields higher low O_2 volumes under new steady state conditions. In brief, hypoxic waters expand over the next millennium across the scenario range and recovery towards modern conditions is slow and in the case of high forcing incomplete. Acknowledging millennial timescales, the hazard of expanding low O_2 waters is much larger than when assessed on the near-term timescale.

~~Simulated changes in export, too, exhibit a distinct temporal evolution. Changes~~ The sensitivity of changes in low latitude export production (30°S - 30°N) is similar at the end of the 21st century ~~scale with -1.2 % °C^{-1} of realized warming and peak changes scale with -0.93~~and at time of peak decline. Changes scale with 2.2 % °C^{-1} ~~of equilibrium temperature response. The global recovery level is similar among the forcings~~. Export production in the low latitudes recovers for lower forcing, but remains reduced in the high forcing case.

~~The metabolic index Φ, as proposed by *Deutsch et al.* (2015), is linear in pO_2 (representing the rate of O_2 supply) and decreases non-linearly with temperature (indicative of the resting metabolic demand). The globally averaged, upper ocean (depth < 400 m) metabolic index declines throughout the simulation dominated by increased temperatures. Decreases~~ Decreases in the metabolic index of the upper ocean scale linearly with forcing: 5.1 % °C^{-1} of realized warming at the end of the 21st century and 6.2 % °C^{-1} of equilibrium temperature response. Likewise, global mean oceanic temperatures increase by 0.099 °C °C^{-1} of realized warming at the end of the 21st century and by 0.56 °C °C^{-1} ~~of equilibriumsurface air temperature response~~at equilibrium. In conclusion, the compound hazards related to deoxygenation and warming, as indicated by the metabolic stress index, evolve over millennia and increase with increasing anthropogenic forcing and with time.

Not only the magnitude or intensity, but also the duration of oxygen related, transient hazards, and thus the severity of the hazards increases with increasing temperature targets. The severity combines magnitude and duration of a hazard in one measure. It may be defined as the time integral of a hazard. The severity of the hazard of expanding hypoxic waters, for example, corresponds to the area under the scenario curve shown in Fig. 2i (the area enclosed by the null line and the modeled evolution, here until the end of the simulation). Fig. 2b,h, and i illustrate that the severity of the three hazards decreasing mean oxygen concentration, expanding hypoxic waters, and reduced export of particulate organic matter providing food for deep sea organisms, increases strongly from low to high temperature targets.

~~Figure 2 further explains the temporal evolution and interplay of the underlying drivers. In all cases, the changes in global oxygen inventory strongly correlate with water mass age and are also impacted by gradual oxygen loss due to warming (Fig. 2e,f). Inventory changes based on the O_2 production tracer are negligible; changes equilibrate with the atmosphere and only a small fraction remains in the ocean. The O_2 consumption tracer determines the shape of the global O_2 signal. It correlates strongly with ideal age and integrates changes in overturning and remineralization fluxes. Changes from remineralization fluxes include both changes in absolute aerobic remineralization fluxes and changes in the relative share of denitrification. An increased share of denitrification at organic matter remineralization, for instance, effectively constitutes an implicit O_2 gain. Denitrification fluxes correlate with the volumetric expansion of OMZs and are also impacted by changes in remineralization fluxes within them (Fig. 2j). O_2 loss due to warming adds to transient decreases in O_2 utilization and diminishes the recovery level. As such, 1.5 to 3.3 °C warming targets reach similar equilibrium levels for different reasons. The degree of increased overturning from additional warming and resulting oxygenation in relation to O_2 loss due to higher temperatures cancel out. The 9.2 °C warming target reaches a lower equilibrium inventory compared to preindustrial due to high O_2 loss from solubility (-44.1 Pmol).~~

~~The decline and recovery pattern in oxygen changes is dominated by changes in overturning. Both Atlantic and Indo-Pacific overturning are projected to slow down and recover. Decline and recovery level as well as the decline and recovery rate vary with forcing level. Generally, Bern3D projects larger slowdown for higher forcing (Fig. 2c,d). The recovery level with forcing differs among AMOC and Indo-Pacific MOC. Higher forcing levels tend to lead to lower recovery for the AMOC and higher recovery levels for the Indo-Pacific MOC. This has direct consequences for the projected global water mass age and by that for oceanic oxygen. The higher the forcing, the higher the transient increase in water mass age. The decrease in global water mass age, which is larger for higher forcing, is dominated by increased Indo-Pacific MOC.~~

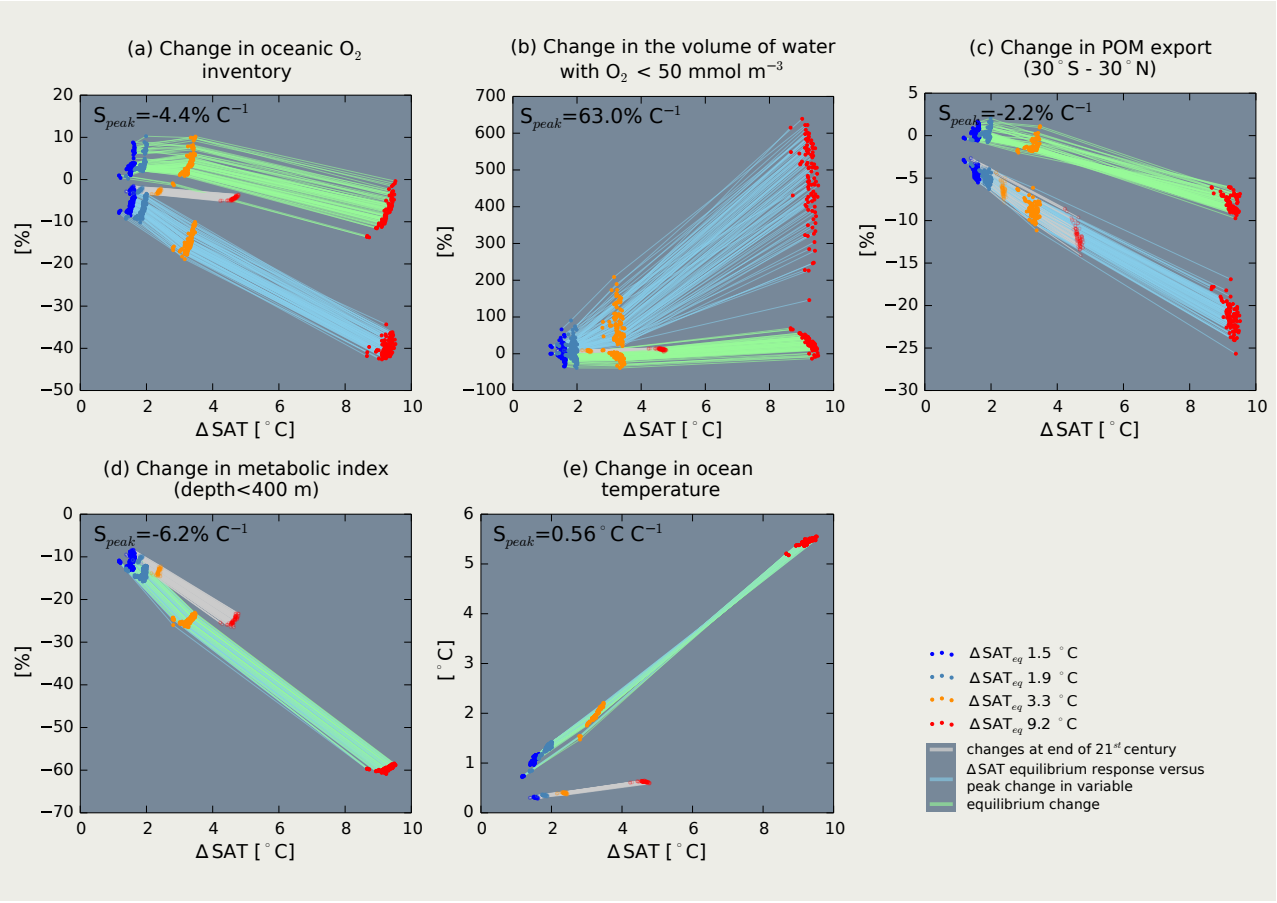

~~emporal evolution of critical variables relative to 1870-1899 for the model ensembles aiming at 1.5, 1.9, 3.3 and 9.2 °C warming targets. Lines mark the median and shading marks the 90 % range of the ensemble. c) Atlantic meridional overturning is the maximum of the Atlantic and d) Indo-Pacific meridional overturning is the minimum of the Indo-Pacific meridional overturning streamfunction below 400 m depth. e) O_{2sat} is the explicitly traced solubility component of oceanic oxygen. i) Oxygen-poor waters are taken as the volume of water with O_2 < 50 mmol m^{-3}.~~

5 ~~Spatial changes in physical and biological variables for a 1.5 °C warming target~~

~~We now address spatial changes in critical variables for a single, representative ensemble member at its peak O_2 decline which occurs at year AD 3150 and amounts to 5 % (Fig. 4). The member eventually reaches a 1.5~~ S_{peak} is the peak sensitivity of each variable per ~~°C warming target. O_2 changes show strong spatial correlation with changes in water mass age (Fig. 4a,b). Despite the global decrease, higher O_2 concentrations are simulated in subsurface waters where ideal age is younger. In near surface waters, local changes in remineralization may contribute to oxygen changes. Below 2 km, overall lower O_2 concentrations are simulated compared to preindustrial. Highest decreases are simulated in bottom waters in line with older water mass age. The presented gradients at peak O_2 decline tend to be more pronounced for higher forcings.~~

~~Export of particulate organic matter is simulated to increase in high latitudes and decrease elsewhere (Fig. 4c). Decreases in export production result from increased stratification and a concomitant increase in nutrient limitation in low latitudes (Fig. 4d, see also *Steinacher et al.* (2009); *Battaglia and Joos* (2017)). The increases in export production in the Arctic and Southern Ocean are due to less temperature and light limitation as surface waters warm and sea ice retreats.~~

~~The temperature anomaly is strongest within the upper ocean and decreases with depth. A pronounced temperature anomaly develops in the~~

5 Uncertainties in O_2 projections~~- including a paleo perspective~~

The pattern and magnitude of simulated global O_2 changes are determined by the response of the overturning circulation. O_2 loss due to less O_2 solubility at higher temperatures gradually decreases oceanic O_2, in addition. ~~In Bern3D, strong deoxygenation in all basins is projected to peak long after the end of the 21st century, after year AD 3000 and new steady state conditions establish after AD 8000. The equilibration timescale of oceanic oxygen is therefore longer than the thermal equilibration timescale of both the atmosphere (~1000 years) and the ocean (~4000 years).~~ Only few multi-millennial simulations with GCMs currently exist. The response of the overturning circulation on long timescales differs among available model simulations (including EMICs and GCMs)~~and Bern3D shows a comparatively strong reduction in Indo-Pacific overturning~~. Uncertainties in the equilibrium climate sensitivity additionally impact projections of O_2 loss due to solubility. These uncertainties directly impact projections of oceanic oxygen.

Similar circulation dynamics as simluated here (Fig. ~~2e,d~~1e,f) were found by *Rugenstein et al.* (2016) based on EMIC simulations ~~(ECBILT-CLIO)~~ over 10,000 years with ECBILT-CLIO, which features a dynamic, quasi-geostrophic atmosphere. *Schmittner et al.* (2008), too, found similar AMOC and Indo-Pacific MOC characteristics for their EMIC ~~(~~UVic 2.7~~)~~, which includes an atmospheric energy balance model with fixed wind fields similar to the Bern3D model, over a 2000 year simulation. *Yamamoto et al.* (2015), on the other hand, found different overturning characteristics in a ~~GCM simulation~~ simulation with a state-of-the art Earth System Model (MIROC 3.2 for a 4xCO_2) over 2000 years. There AMOC slowed down with no recovery, while AABW decreased only slightly and gradually increased thereafter. Predictions of AMOC have received more attention so far, and AMOC slowdown and partial or full recovery emerges in other multi-millennial simulations (*Zickfeld et al.*, 2013; *Li et al.*, 2013; *Weaver et al.*, 2012). AMOC and Southern Ocean overturning in CMIP5 ~~models~~ Earth System Models was analyzed by *Heuzé et al.* (2015). They found AMOC and Southern Ocean overturning is positively correlated in most CMIP5 models by the end of the 21st century. Generally, preindustrial circulation states, magnitudes and timing of changes are highly model and scenario dependent such that the long-term evolution of meridional overturning is uncertain. As oxygen changes are dominated by circulation changes, this makes the oxygen prediction highly model and scenario dependent, as well. The simulated timing and strength of peak O_2 decrease in Bern3D is similar to what *Schmittner et al.* (2008, AD 3000, 30 % for SRES A2 high emission scenario/SAT$\sim$10 °C in Uvic 2.7) found. Other comparable simulations show earlier peaks and smaller magnitudes (*Mathesius et al.* (2015, AD 2600, 16 % decrease for RCP8.5/ΔSAT$\sim$7 °C in CLIMBER-3α), *Yamamoto et al.* (2015, after 800 model years, 10 % for 4xCO_2/ΔSAT$\sim$8.5 °C in MIROC 3.2).

~~Paleo proxies suggest oceanic oxygen concentrations have undergone large climate-driven changes in the past (*Jaccard et al.*, 2014; *Jacc*~~
~~The deglacial warming of about 3 to 4 °C from the Last Glacial Maximum to the Holocene (*Shakun et al.*, 2012), for instance, has led to oxygenation of the oceans (*Jaccard et al.*, 2014) similar to our model simulations producing 1.5 to 3.3 °C warming above preindustrial. Analogies between reconstructed past and simulated future climate change therefore exist for the respective equilibrium states. Trends at the end of the 21st century, however, are opposite to such expectations. Proxies of past ocean~~

oxygenation and ventilation reveal similar structural changes and mechanisms. Increases in overturning from the LGM to the Holocene are thought to have increased deep oxygen levels and higher temperatures are thought to have decreased O_2 in the upper ocean due to less solubility (*Jaccard et al.*, 2014). The process attribution for both paleo proxies and our long term Earth System projections including 1.5 to 3.3 °C warming targets are therefore similar. For very large radiative forcing and climate change, such as realized in the RCP8.5 scenario, projected ocean oxygen, however, remains below current concentrations even after reaching a new equilibrium. In Bern3D, changes in ventilation generally outweigh changes in remineralization fluxes as actual driver of oxygen changes. For example, oxygen concentrations decrease in the deep ocean of the low latitude and North Pacific despite lower remineralization fluxes there. At intermediate depth, younger water masses and reduced remineralization fluxes contribute to higher O_2 concentrations. This is in contrast to the mechanisms of O_2 changes identified by *Praetorius et al.* (2015) for the last deglacial transition. They postulate abrupt warming triggered expansion of the North Pacific OMZ at intermediate depth through reduced oxygen solubility and increased productivity there. We note, however, that close comparisons across the different climate states and different climate evolutions remain tentative

Major physical limitations of our simulations concern prescribed winds and ice-sheets. Future model studies may include sensitivity simulations with prescribed changes in the wind stress over the ocean (e.g. *Tschumi et al.*, 2008) and prescribed meltwater fluxes or apply earth system models with interactive atmospheric dynamics and ice sheets. Our study, as is the case for most climate change simulations, do not include melting of continental ice sheets, which would tend to further (transiently) reduce circulation (*Bakker et al.*, 2016) and increase the equilibrium climate sensitivity.

Current generation GCMs, such as is the case for Bern3D, have difficulty simulating the current distribution of OMZs due to missing physical processes operating at small spatial scales, such as eddies and zonal jets (*Cocco et al.*, 2013; *Bopp et al.*, 2013) or missing biogeochemical characteristics. Large model-data and model-model discrepancies exist (*Bopp et al.*, 2013). *Laufkötter et al.* (2017) recently achieved improved representation of OMZs introducing temperature and oxygen dependence of the remineralization profile within a GCM (GFDL ESM2M). In our ensemble, the magnitude of peak increases in low O_2 waters depend strongly on the rate of organic matter remineralization. Temperature dependent feedback mechanisms, neglected here, may be addressed in future studies. Both particulate sinking speed and local remineralization rates, which control the remineralization profile, have been shown to be sensitive to temperature. While higher temperatures increase bacterial activity and therefore remineralization (*Bendtsen et al.*, 2014) they decrease viscosity and therefore increase sinking speed (*Taucher et al.*, 2014). The net effect on the remineralization profile is correspondingly uncertain. In addition, ecosystem structure influences the size and density of organic particles available for export (*Armstrong et al.*, 2001, 2009). Given these existing uncertainties and the coarse resolution physical models, the projections of OMZs has to be viewed with caution. The general sense of change, that low O_2 waters expand with warmer equilibrium climate states as inferred from proxy observations (*Jaccard et al.*, 2014) is not simulated by the ensembles reaching 1.5 and 3.3 °C warming targets. Despite simulated lower background concentrations of O_2 in the subsurface ocean, the volumes of low O_2 waters decrease for steady state conditions

in the model. ~~It remains to be explored whether this difference is related to deficiencies in the ocean model or in proxy data or related to the different climate states covered by the proxy data (last glacial termination) and the model simulations.~~

We neglect a number of biogeochemical feedback mechanisms that could alter biological productivity in the surface ocean and by that change remineralization fluxes in the water column. Any mechanisms that would increase remineralization would tend to decrease the oceanic oxygen, and mechanisms that decrease remineralization would increase the oceanic oxygen content. Future studies may address feedbacks from sediment interactions and imbalances from riverine input and burial (such as *Roth et al.*, 2014; *Niemeyer et al.*, 2017), temperature dependent remineralization, and variable stoichiometry. Further investigations may also address nitrogen cycle dynamics and assess the interplay of denitrification and N-fixation and of external atmospheric and terrestrial nitrogen sources. The resulting impact on the fixed nitrogen inventory in the ocean are currently unclear.

6 Implications and Conclusion

In Bern3D, strong deoxygenation in all basins is projected to peak long after the end of the 21st century, and new steady state conditions establish after AD 8000 in scenarios where radiative forcing is stabilized in the next century. The equilibration timescale of oceanic oxygen is therefore longer than the thermal equilibration timescale of both the atmosphere (∼1000 years) and the ocean (∼4000 years). Based on CMIP5 models, *Sweetman et al.* (2017) discuss the deep-sea ecosystem implications of climate change by 2100. Deep sea ecosystems provide a range of services from habitat provision, nursery grounds, trophic support, refugia to biodiversity (reviewed in *Sweetman et al.*, 2017). Biogeochemical changes such as deoxygenation, warming, acidification and less food availability will likely be accompanied by exploitation of mineral resources, over fishing and dumping of pollutants and microplastics. We project largest biogeochemical changes beyond 2100 and to aggravate over millennia. How these changes will affect deep-sea ecosystems is poorly understood. The adaptation to stress may be limited by slow growth rates and long generation times of deep sea ecosystems (*Sweetman et al.*, 2017).

Figure 6a contrasts ~~transient~~ near-term (A.D. 2100) and peak changes (relative to 1870-1899) in measures of metabolically viable habitats in the upper ocean, hypoxia, and food availability as projected by Bern3D for a 1.5°C warmer world. Export in low latitudes (30°S - 30°N) as an indicator of food availability is reduced by maximally 4% over the course of the simulation in this scenario. Median decreases in the metabolic index, representing viable habitat reductions of the upper ocean, amount to 11 % for a 1.5° warmer world. The volume of low oxygen waters is particularly sensitive to anthropogenic warming ~~. While export production, as an indicator of food availability, changes only by some percent, the~~ and peak changes occur after the end of the 21st century. The volume of water with $O_2 < 50$ mmol m^{-3} changes by 6.6 % by the end of the century and by 14 % ~~. Median decreases in the metabolic index, representing viable habitat reductions of the upper ocean, amount to 11 % for a~~ at its peak. Meeting the 1.5° ~~warmer world.~~ C climate target of the Paris Agreement requires very fast and very stringent emission reductions (*Steinacher et al.*, 2013; *Sanderson et al.*, 2016; *Millar et al.*, 2017). Estimates by *Steinacher et al.* (2013) for a range of scenarios show that post-2017 allowable carbon emissions from fossil fuel need to be lower than 320 GtC to meet the 1.5°C target with 66% probability. This corresponds in the most optimistic scenario to only slightly more than three decades of current fossil fuel use. The Nationally Determined Contribution, outlining emission mitigation actions by the Parties of the Paris Agreement, need to be strengthened in ambition and scope to meet the 1.5°C or the 2°C target (*Joeri et al.*, 2016). Such efforts would lead not only to lower warming compared to the current emission trajectory, but also have the benefit of reduced marine hazards as investigated here (Fig. 6b).

Higher temperature targets increase the hazard of ecosystem impacts as expressed in the ~~chosen~~ investigated variables. In particular, measures of peak hypoxia exhibit a strong sensitivity to additional warming (Fig. ~~-~~6b).

~~Projected peak losses~~ Measures of deoxygenation, marine food scarcity, and marine aerobic habitat reduction are aggravated for the 2°C compared to the 1.5°C temperature target and investigated hazards are strongly amplified in a world where surface

air temperature is stabilized at 3.3°C (Fig. 6b). Unbounded use of carbon emissions from existing fossil resources is projected not only to lead to a global warming of order 10°C (Fig. 1a, Fig. 4; *Randerson et al.*, 2015; *Zickfeld et al.*, 2013), but also to a peak reduction in global mean ~~O_2 scale linearly with forcing such that more stringent~~ oxygen inventory by almost a factor of two (Fig. 2a, Fig. 4a).

We find close to linear relationship between impact-relevant marine hazards and global mean surface air temperature. This allows us to quantify avoided hazards per unit of avoided global warming. For example, emission mitigation measures would help to reduce peak O_2 loss by 4.4 % $°C^{-1}$ of avoided equilibrium warming. ~~At peak O_2 loss, deep-sea environments are projected to be prone to largest changes: Large O_2 loss and slight warming contribute to less metabolic viability. Potential metabolic benefit from increased O_2 concentrations, which may develop at peak O_2 loss in subsurface waters, are offset by increased temperatures in most places. After transient deoxygenation, the future oceanic oxygen inventory in a 1.5 to 3.3 °C warmer world may well exceed preindustrial conditions. Under new steady state conditions, increased metabolic indices develop in better ventilated waters of the Southern Ocean and deep Indo-Pacific, despite higher temperatures. Yet, under high anthropogenic emissions and forcings such as projected in the RCP8.5 scenario, the total ocean oxygen inventory and metabolic viability is reduced compared to today.~~

The Earth system response timescale to climate change spans several millennia such that anthropogenic perturbations to greenhouse-gas concentrations commit the Earth system to long-term, irreversible climate change (*Clark et al.*, 2016). Our simulations show that the long-term fate of oceanic oxygen is characterized by an initial decline followed by a recovery phase. Peak decline and associated potential adverse ecosystem impacts are projected long after stabilization of radiative forcing in the atmosphere. This adds to the list of long-term Earth System commitments including warming, acidification and sea-level rise assessed elsewhere ~~(*Eby et al.*, 2009; *Lord et al.*, 2016; *Pfister and Stocker*, 2016; *Clark et al.*, 2016)~~(*Eby et al.*, 2009; *Ridgwell and Schmidt*
Long-term, multi-millennial perspectives are thus required for a full account of climate-related ocean risks.

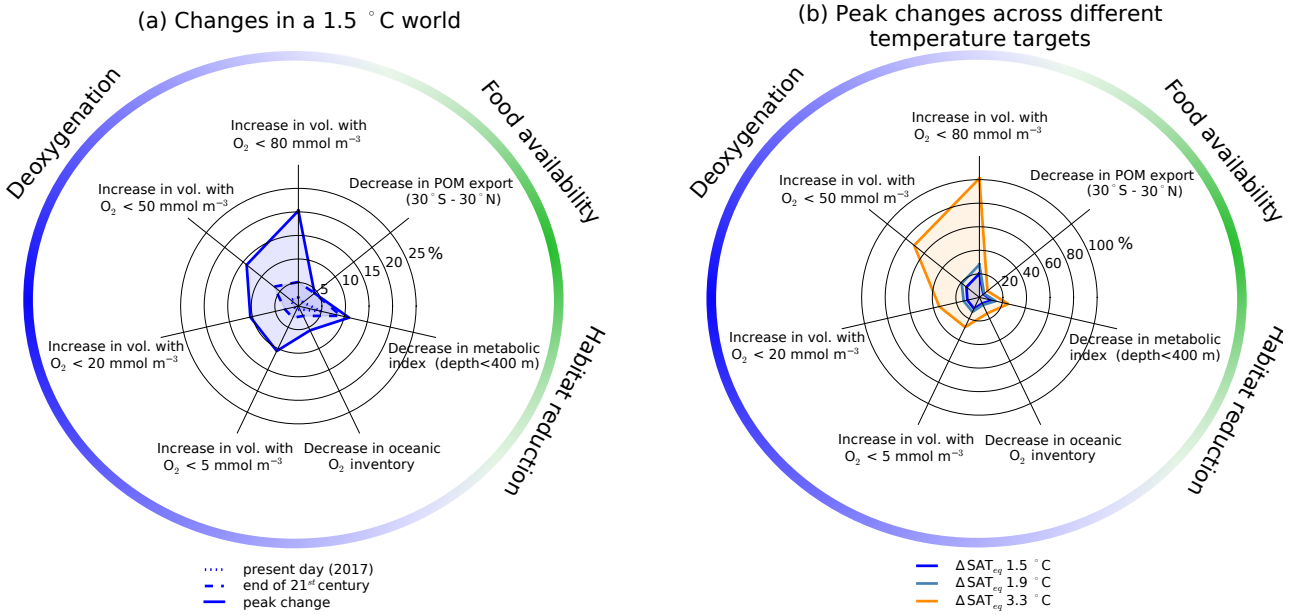

Figure 6. Contrasting hazards of ecosystem impacts expressed in measures of hypoxia, metabolic viability of the upper ocean, and food availability. a) Changes for a 1.5 °C warmer world at present, at the end of the century and compared to peak changes. b) Peak changes across 1.5, 1.9 and 3.3 °C temperature targets. Lines correspond to the median response across each ensemble relative to 1870-1899.

Data availability. Model output is available upon request to the corresponding author (battaglia@climate.unibe.ch).

Appendix A: Spatial properties of a representative ensemble member reaching a 1.5°C warming target

In this appendix we document additional spatial properties of the representative ensemble member reaching a 1.5°C warming target. Figure A1 illustrates the meridional overturning streamfunction for PI, year A.D. 2050 where the AMOC is at its lowest value, and for new steady state conditions. Figure A2 illustrates the evolution of temperature, salinity, and density anomalies across a transect from the Atlantic Ocean, through the Southern Ocean and into the Pacific at A.D. 2100, A.D. 3150 when the O_2 inventory is at its lowest values, and for new steady state conditions. Figure A3 shows the anomalies in total O_2 and the contributions from biology and solubility components for new steady conditions relative to PI. In addition, anomalies in ideal age are shown.

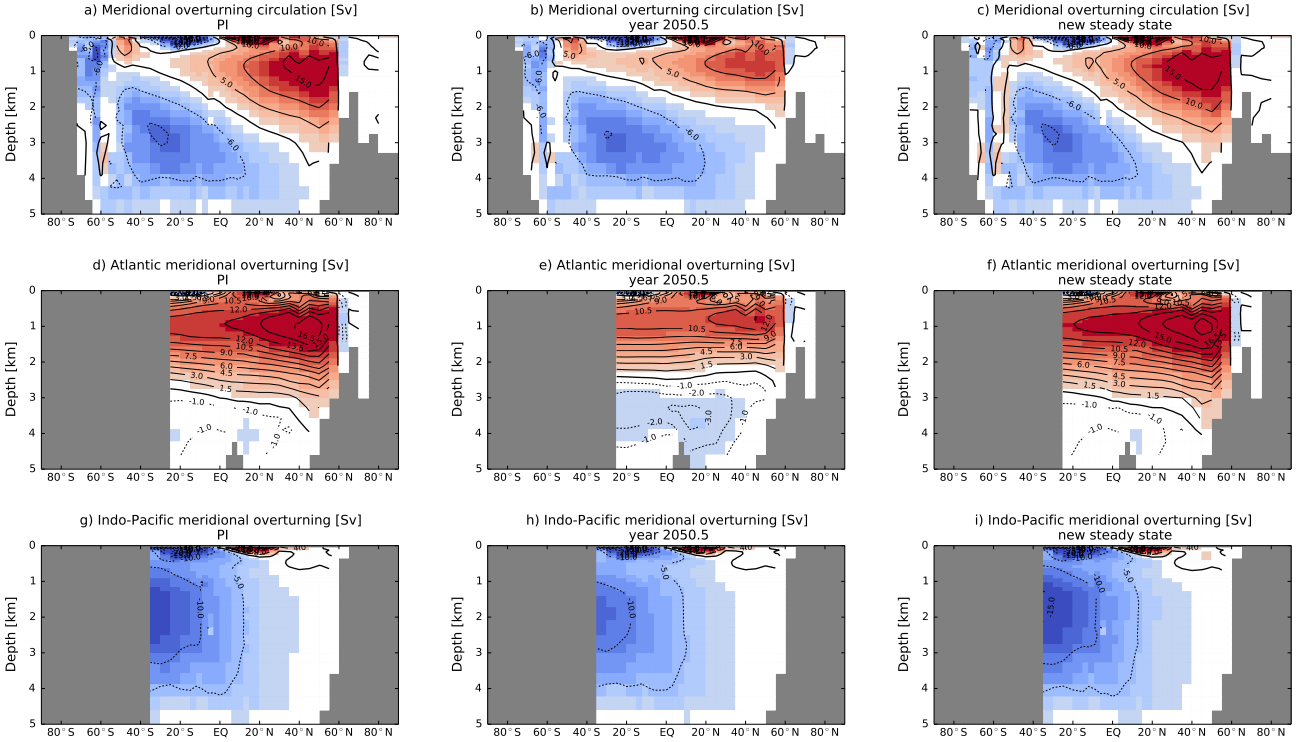

Figure A1. Meridional overturning streamfunction in (a-c) the world ocean, (d-f) Atlantic ocean, and (g-i) Indo-Pacific for PI, year 2050, and for new steady state conditions for a representative ensemble member reaching a 1.5°C warming target (columns). Circulation is clockwise along positive (red) contours and anticlockwise along the negative (blue) contours.

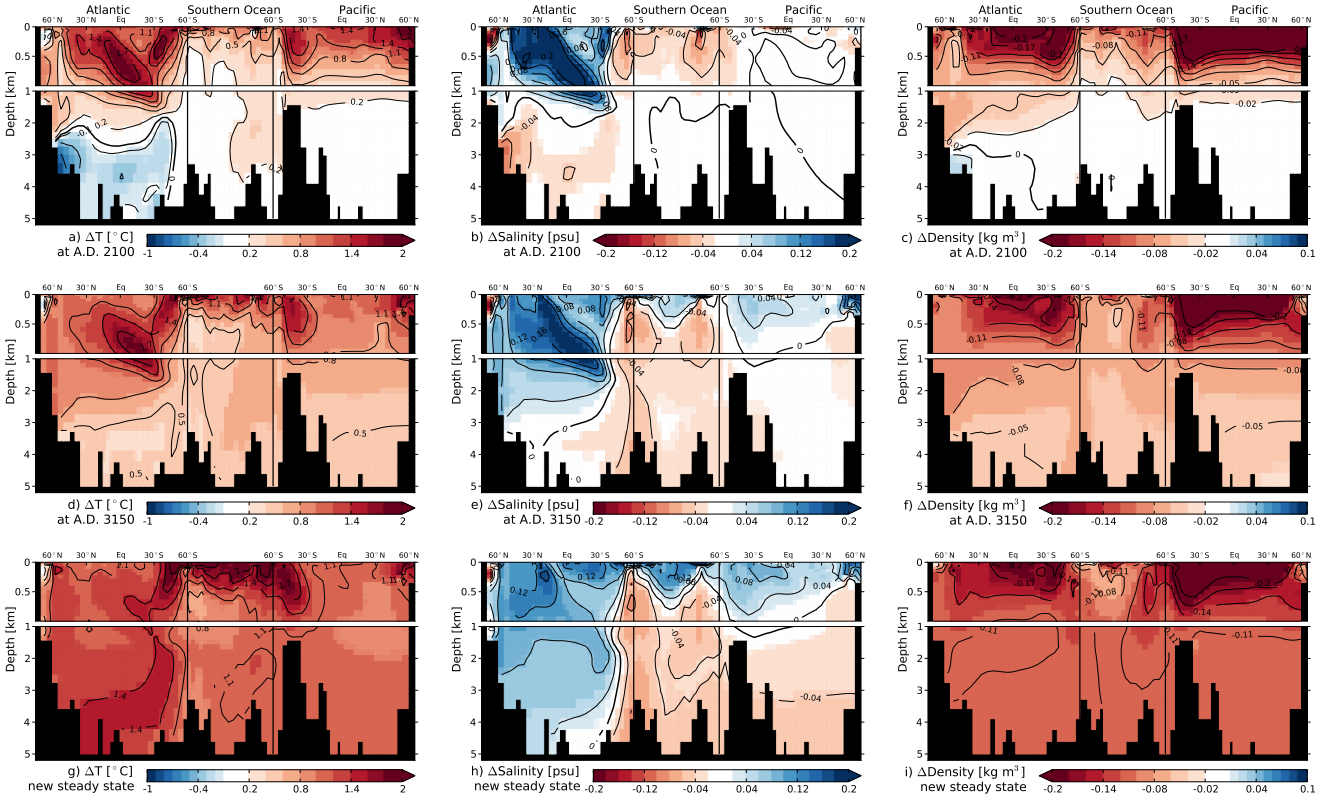

Figure A2. Changes in temperature, salinity and density at A.D. 2100 (a,b,c), at A.D. 3150 (d,e,f), and for new steady state conditions (g,h,i) compared to pre-industrial conditions.

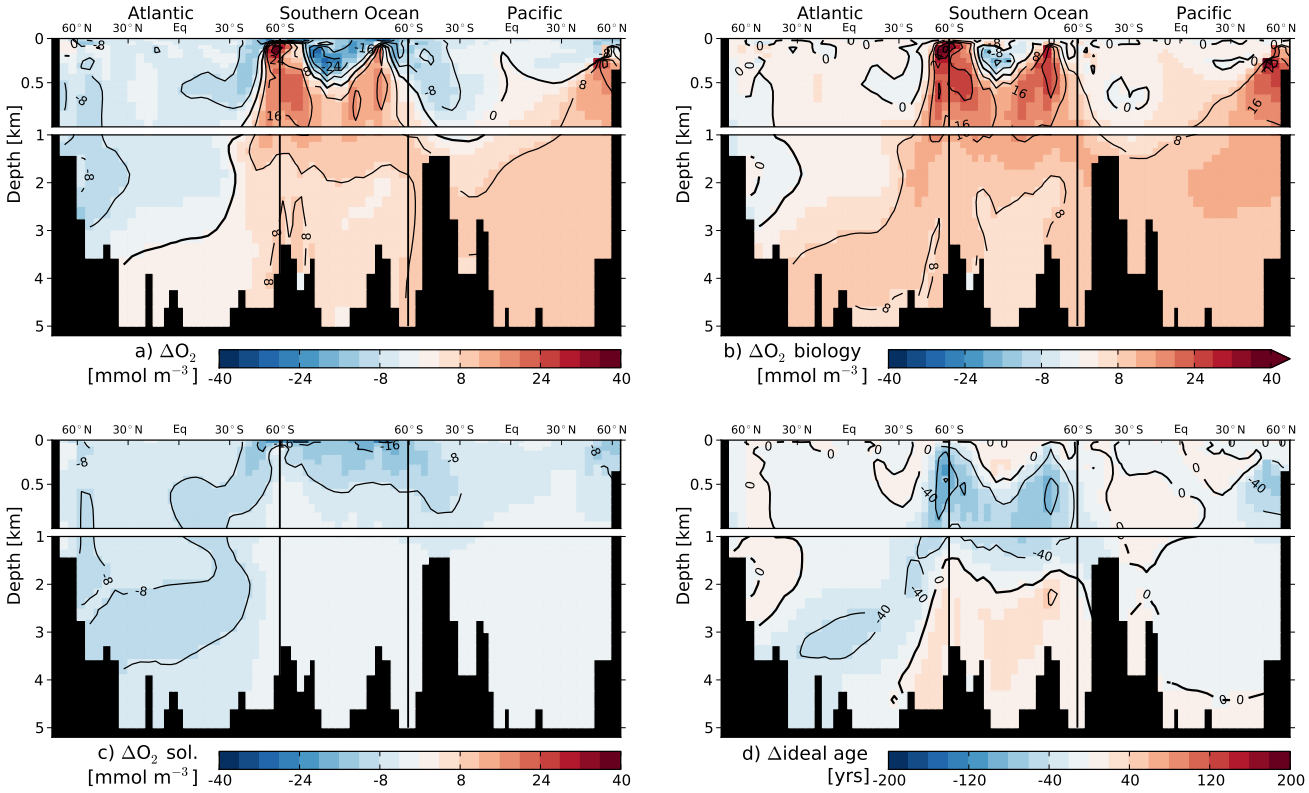

Figure A3. Changes in O_2 and its components for new steady state conditions relative to preindustrial steady state for a single, representative ensemble member reaching a 1.5 °C warming target. a) Change in total O_2, b) change in O_2 due to biology, c) change in O_2 due to solubility, d) changes in ideal age.

Competing interests. The authors declare that they have no conflict of interest.

Acknowledgements. We thank Patrik Pfister, and Thomas Frölicher ~~and Andreas Oschlies~~ for fruitful discussions. This work was supported by the Swiss National Science Foundation (200020_172476).

References

Allen, M. R., D. J. Frame, C. Huntingford, C. D. Jones, J. A. Lowe, M. Meinshausen, and N. Meinshausen (2009), Warming caused by cumulative carbon emissions towards the trillionth tonne, *Nature*, *458*, 1163.

Armstrong, R. A., C. Lee, J. I. Hedges, S. Honjo, and S. G. Wakeham (2001), A new, mechanistic model for organic carbon fluxes in the ocean based on the quantitative association of POC with ballast minerals, *Deep Sea Research Part II: Topical Studies in Oceanography*, *49*(1), 219–236, doi:10.1016/S0967-0645(01)00101-1, the US JGOFS Synthesis and Modeling Project: Phase 1.

Armstrong, R. A., M. L. Peterson, C. Lee, and S. G. Wakeham (2009), Settling velocity spectra and the ballast ratio hypothesis, *Deep Sea Research Part II: Topical Studies in Oceanography*, *56*(18), 1470–1478, doi:10.1016/j.dsr2.2008.11.032, medFlux:Investigations of Particle Flux in the Twilight Zone.

Bakker, P., A. Schmittner, J. T. M. Lenaerts, A. Abe-Ouchi, D. Bi, M. R. van den Broeke, W.-L. Chan, A. Hu, R. L. Beadling, S. J. Marsland, S. H. Mernild, O. A. Saenko, D. Swingedouw, A. Sullivan, and J. Yin (2016), Fate of the Atlantic Meridional Overturning Circulation: Strong decline under continued warming and Greenland melting, *Geophysical Research Letters*, *43*(23), 12,252–12,260.

Battaglia, G., and F. Joos (2017), Marine N2O emissions from nitrification and denitrification constrained by modern observations and projected under large anthropogenic deoxygenation, *Global Biogeochemical Cycles*, *in review*.

Battaglia, G., and F. Joos (2018), Marine N2O Emissions From Nitrification and Denitrification Constrained by Modern Observations and Projected in Multimillennial Global Warming Simulations, *Global Biogeochemical Cycles*.

Battaglia, G., M. Steinacher, and F. Joos (2016), A probabilistic assessment of calcium carbonate export and dissolution in the modern ocean, *Biogeosciences*, *13*(9), 2823–2848, doi:10.5194/bg-13-2823-2016.

Bendtsen, J., K. M. Hilligsøe, J. L. Hansen, and K. Richardson (2014), Analysis of remineralisation, lability, temperature sensitivity and structural composition of organic matter from the upper ocean, *Progress in Oceanography*, doi:10.1016/j.pocean.2014.10.009.

Bianchi, D., J. P. Dunne, J. L. Sarmiento, and E. D. Galbraith (2012), Data-based estimates of suboxia, denitrification, and N2O production in the ocean and their sensitivities to dissolved O2, *Global Biogeochem. Cycles*, *26*(2), GB2009, doi:10.1029/2011gb004209.

Bopp, L., C. Le Quéré, M. Heimann, A. C. Manning, and P. Monfray (2002), Climate-induced oceanic oxygen fluxes: Implications for the contemporary carbon budget, *Global Biogeochemical Cycles*, *16*(2), 6–1–6–13.

Bopp, L., L. Resplandy, J. C. Orr, S. C. Doney, J. P. Dunne, M. Gehlen, P. Halloran, C. Heinze, T. Ilyina, R. Séférian, J. Tjiputra, and M. Vichi (2013), Multiple stressors of ocean ecosystems in the 21st century: projections with CMIP5 models, *Biogeosciences*, *10*(10), 6225–6245, doi:10.5194/bg-10-6225-2013.

Bopp, L., L. Resplandy, A. Untersee, P. Le Mezo, and M. Kageyama (2017), Ocean (de)oxygenation from the Last Glacial Maximum to the twenty-first century: insights from Earth System models, *Philosophical Transactions of the Royal Society of London A: Mathematical, Physical and Engineering Sciences*, *375*(2102), doi:10.1098/rsta.2016.0323.

Breitburg, D., L. A. Levin, A. Oschlies, M. Grégoire, F. P. Chavez, D. J. Conley, V. Garçon, D. Gilbert, D. Gutiérrez, K. Isensee, G. S. Jacinto, K. E. Limburg, I. Montes, S. W. A. Naqvi, G. C. Pitcher, N. N. Rabalais, M. R. Roman, K. A. Rose, B. A. Seibel, M. Telszewski, M. Yasuhara, and J. Zhang (2018), Declining oxygen in the global ocean and coastal waters, *Science*, *359*(6371), doi:10.1126/science.aam7240.

Cabre, A., I. Marinov, R. Bernardello, and D. Bianchi (2015), Oxygen minimum zones in the tropical Pacific across CMIP5 models: Mean state differences and climate change trends, *Biogeosciences*, *12*(18), 5429–5454, doi:10.5194/bg-12-5429-2015.

Cheung, W. W. L., G. Reygondeau, and T. L. Frölicher (2016), Large benefits to marine fisheries of meeting the 1.5°C global warming target, *Science*, *354*(6319), 1591–1594, doi:10.1126/science.aag2331.

Clark, P. U., J. D. Shakun, S. A. Marcott, A. C. Mix, M. Eby, S. Kulp, A. Levermann, G. A. Milne, P. L. Pfister, B. D. Santer, D. P. Schrag, S. Solomon, T. F. Stocker, B. H. Strauss, A. J. Weaver, R. Winkelmann, D. Archer, E. Bard, A. Goldner, K. Lambeck, R. T. Pierrehumbert, and G.-K. Plattner (2016), Consequences of twenty-first-century policy for multi-millennial climate and sea-level change, *Nature Climate Change*, *6*(4), 360–369, doi:10.1038/nclimate2923.

Cocco, V., F. Joos, M. Steinacher, T. L. Frölicher, L. Bopp, J. Dunne, M. Gehlen, C. Heinze, J. Orr, A. Oschlies, B. Schneider, J. Segschneider, and J. Tjiputra (2013), Oxygen and indicators of stress for marine life in multi-model global warming projections, *Biogeosciences*, *10*(3), 1849–1868, doi:10.5194/bg-10-1849-2013.

Deutsch, C., A. Ferrel, B. Seibel, H.-O. Pörtner, and R. B. Huey (2015), Climate change tightens a metabolic constraint on marine habitats, *Science*, *348*(6239), 1132–1135, doi:10.1126/science.aaa1605.

Diaz, R. J., and R. Rosenberg (2008), Spreading Dead Zones and Consequences for Marine Ecosystems, *Science*, *321*(5891), 926–929, doi:10.1126/science.1156401.

Doney, S. C., K. Lindsay, I. Fung, and J. John (2006), Natural Variability in a Stable, 1000-yr Global Coupled Climate–Carbon Cycle Simulation, *J. Climate*, *19*(13), 3033–3054, doi:10.1175/JCLI3783.1.

Eby, M., K. Zickfeld, A. Montenegro, D. Archer, K. J. Meissner, and A. J. Weaver (2009), Lifetime of Anthropogenic Climate Change: Millennial Time Scales of Potential CO2 and Surface Temperature Perturbations, *Journal of Climate*, *22*(10), 2501–2511, doi:10.1175/2008JCLI2554.1.

Ehlert, D., and K. Zickfeld (2017), What determines the warming commitment after cessation of CO2 emissions?, *Environmental Research Letters*, *12*(1), 015,002.

Frölicher, T. L., F. Joos, G.-K. Plattner, M. Steinacher, and S. C. Doney (2009), Natural variability and anthropogenic trends in oceanic oxygen in a coupled carbon cycle–climate model ensemble, *Global Biogeochemical Cycles*, *23*(1), doi:10.1029/2008GB003316, gB1003.

Garcia, H. E., R. A. Locarnini, T. P. Boyer, J. I. Antonov, O. K. Baranova, M. M. Zweng, J. R. Reagan, and D. R. Johnson (2014), World Ocean Atlas 2013, Volume 3: Dissolved Oxygen, Apparent Oxygen Utilization, and Oxygen Saturation, *NOAA Atlas NESDIS 75 75*.

Gattuso, J.-P., A. Magnan, R. Billé, W. W. L. Cheung, E. L. Howes, F. Joos, D. Allemand, L. Bopp, S. R. Cooley, C. M. Eakin, O. Hoegh-Guldberg, R. P. Kelly, H.-O. Pörtner, A. D. Rogers, J. M. Baxter, D. Laffoley, D. Osborn, A. Rankovic, J. Rochette, U. R. Sumaila, S. Treyer, and C. Turley (2015), Contrasting futures for ocean and society from different anthropogenic CO2 emissions scenarios, *Science*, *349*(6243), doi:10.1126/science.aac4722.

Golledge, N. R., D. E. Kowalewski, T. R. Naish, R. H. Levy, C. J. Fogwill, and E. G. W. Gasson (2015), The multi-millennial Antarctic commitment to future sea-level rise, *Nature*, *526*(7573), 421–425, doi:10.1038/nature15706.

Gruber, N. (2011), Warming up, turning sour, losing breath: ocean biogeochemistry under global change, *Philos. T. R. Soc. A*, *369*(1943), 1980–1996, doi:10.1098/rsta.2011.0003.

Heuzé, C., K. J. Heywood, D. P. Stevens, and J. K. Ridley (2015), Changes in Global Ocean Bottom Properties and Volume Transports in CMIP5 Models under Climate Change Scenarios, *Journal of Climate*, *28*(8), 2917–2944, doi:10.1175/JCLI-D-14-00381.1.

Hofmann, M., and H.-J. Schellnhuber (2009), Oceanic acidification affects marine carbon pump and triggers extended marine oxygen holes, *Proceedings of the National Academy of Sciences*, *106*(9), 3017–3022, doi:10.1073/pnas.0813384106.

IPCC (2013), Climate Change 2013: The Physical Science Basis. Contribution of Working Group I to the Fifth Assessment Report of the Intergovernmental Panel on Climate Change , p. 1535 pp, Cambridge Univ. Press, United Kingdom and New York, NY, USA, doi:10.1038/446727a.

Ito, T., M. J. Follows, and E. A. Boyle (2004), Is AOU a good measure of respiration in the ocean? , *Geophys. Res. Lett.*, *31*.

Ito, T., S. Minobe, M. C. Long, and C. Deutsch (2017), Upper ocean O2 trends: 1958–2015, *Geophysical Research Letters*, *44*(9), 4214–4223.

Jaccard, S., E. D. Galbraith, T. L. Frölicher, and N. Gruber (2014), Ocean (De)oxygenation Across the Last Deglaciation: Insights for the Future, *Oceanography*, *27*.

Jaccard, S. L., and E. D. Galbraith (2012), Large climate-driven changes of oceanic oxygen concentrations during the last deglaciation, *Nature Geosci*, *5*(2), 151–156, doi:10.1038/ngeo1352, 10.1038/ngeo1352.

Jaccard, S. L., E. D. Galbraith, A. Martínez-García, and R. F. Anderson (2016), Covariation of deep Southern Ocean oxygenation and atmospheric CO2 through the last ice age, *Nature*, *530*(7589), 207–210.

Joeri, R., d. E. Michel, H. Niklas, F. Taryn, F. Hanna, W. Harald, S. Roberto, S. Fu, R. Keywan, and M. Malte (2016), Paris Agreement climate proposals need a boost to keep warming well below 2 °C, *Nature*, *534*, 631.

Joos, F., and R. Spahni (2008), Rates of change in natural and anthropogenic radiative forcing over the past 20,000 years, *P. Natl. Acad. Sci. USA*, *105*(5), 1425–1430, doi:10.1073/pnas.0707386105.

Kalnay, E., M. Kanamitsu, R. Kistler, W. Collins, D. Deaven, L. Gandin, M. Iredell, S. Saha, G. White, J. Woollen, Y. Zhu, M. Chelliah, W. Ebisuzaki, W. Higgins, J. Janowiak, K. C. Mo, C. Ropelewski, J. Wang, A. Leetmaa, R. Reynolds, R. Jenne, and D. Joseph (1996), The NCEP/NCAR 40-year reanalysis project, *B. Am. Meteorol. Soc.*, *77*(3), 437–471, doi:10.1175/1520-0477(1996)077<0437:TNYRP>2.0.CO;2.

Keeling, R. F., A. Körtzinger, and N. Gruber (2010), Ocean Deoxygenation in a Warming World, *Annual review of marine science*, *2*, 199–229.

Key, R. M., A. Kozyr, C. L. Sabine, K. Lee, R. Wanninkhof, J. L. Bullister, R. A. Feely, F. J. Millero, C. Mordy, and T.-H. Peng (2004), A global ocean carbon climatology: Results from Global Data Analysis Project (GLODAP), *Global Biogeochem. Cy.*, *18*(4), GB4031, doi:10.1029/2004GB002247.

Laufkötter, C., J. G. John, C. A. Stock, and J. P. Dunne (2017), Temperature and oxygen dependence of the remineralization of organic matter, *Global Biogeochemical Cycles*, doi:10.1002/2017GB005643, 2017GB005643.

Li, C., J.-S. von Storch, and J. Marotzke (2013), Deep-ocean heat uptake and equilibrium climate response, *Climate Dynamics*, *40*(5), 1071–1086, doi:10.1007/s00382-012-1350-z.

Lord, N. S., A. Ridgwell, M. C. Thorne, and D. J. Lunt (2016), An impulse response function for the "long tail" of excess atmospheric CO2 in an Earth system model, *Global Biogeochemical Cycles*, *30*(1), 2–17, doi:10.1002/2014GB005074, 2014GB005074.

Magnan, A. K., M. Colombier, R. Billé, F. Joos, O. Hoegh-Guldberg, H.-O. Pörtner, H. Waisman, T. Spencer, and J.-P. Gattuso (2016), Implications of the Paris agreement for the ocean, *Nature Climate Change*, *6*(8), 732–735, doi:10.1038/nclimate3038.

Martin, J. H., G. A. Knauer, D. M. Karl, and W. Broenkow (1987), VERTEX: Carbon cycling in the northeast Pacific, *Deep-Sea Res.*, doi:10.1016/0198-0149(87)90086-0.

Matear, R. J. (2000), Climate change impacts on marine systems, *Aust. Microbiol.*, *21(2)*, 17 – 20.

Matear, R. J., and A. C. Hirst (2003), Long-term changes in dissolved oxygen concentrations in the ocean caused by protracted global warming, *Global Biogeochemical Cycles*, *17*(4), doi:10.1029/2002GB001997, 1125.

Mathesius, S., M. Hofmann, K. Caldeira, and J. Schellnhuber Hans (2015), Long-term response of oceans to CO2 removal from the atmosphere, *Nature Clim. Change*, *5*(12), 1107–1113.

McKay, M. D., R. J. Beckman, and W. J. Conover (1979), A comparison of three methods for selecting values of input variables in the analysis of output from a computer code , *Technometrics*, *21*, 239–245.

Meinshausen, M., S. Smith, K. Calvin, J. Daniel, M. Kainuma, J.-F. Lamarque, K. Matsumoto, S. Montzka, S. Raper, K. Riahi, A. Thomson, G. Velders, and D. P. van Vuuren (2011), The RCP greenhouse gas concentrations and their extensions from 1765 to 2300, *Climatic Change*, *109*(1), 213–241, doi:10.1007/s10584-011-0156-z.

Millar, R. J., J. S. Fuglestvedt, P. Friedlingstein, J. Rogelj, M. J. Grubb, H. D. Matthews, R. B. Skeie, P. M. Forster, D. J. Frame, and M. R. Allen (2017), Emission budgets and pathways consistent with limiting warming to 1.5 °C, *Nature Geoscience*, *10*, 741.

Mislan, K. A. S., C. A. Deutsch, R. W. Brill, J. P. Dunne, and J. L. Sarmiento (2017), Projections of climate-driven changes in tuna vertical habitat based on species-specific differences in blood oxygen affinity, *Global Change Biology*, *23*(10), 4019–4028, doi:10.1111/gcb.13799.

Müller, S. A., F. Joos, N. R. Edwards, and T. F. Stocker (2006), Water mass distribution and ventilation time scales in a cost-efficient, three-dimensional ocean model, *J. Climate*, *19*(21), 5479–5499, doi:10.1175/JCLI3911.1.

Müller, S. A., F. Joos, N. R. Edwards, and T. F. Stocker (2008), Modeled natural and excess radiocarbon: Sensitivities to the gas exchange formulation and ocean transport strength, *Global Biogeochem. Cy.*, *22*(GB3011), 14 pp, doi:10.1029/2007GB003065.

Najjar, R. G., J. Orr, C. L. Sabine, and F. Joos (1999), Biotic-HOWTO. Internal OCMIP Report, *Tech. rep.*, LSCE/CEA Saclay, Gif-sur-Yvette, France.

Niemeyer, D., T. P. Kemena, K. J. Meissner, and A. Oschlies (2017), A model study of warming-induced phosphorus–oxygen feedbacks in open-ocean oxygen minimum zones on millennial timescales, *Earth System Dynamics*, *8*(2), 357–367, doi:10.5194/esd-8-357-2017.

Orr, J., and R. G. Najjar (1999), Abiotic-HOWTO. Internal OCMIP Report, *Tech. rep.*, LSCE/CEA Saclay, Gif-sur-Yvette, France.

Orr, J. C., and J.-M. Epitalon (2015), Improved routines to model the ocean carbonate system: mocsy 2.0, *Geoscientific Model Development*, *8*(3), 485–499, doi:10.5194/gmd-8-485-2015.

Oschlies, A., O. Duteil, J. Getzlaff, W. Koeve, A. Landolfi, and S. Schmidtko (2017), Patterns of deoxygenation: sensitivity to natural and anthropogenic drivers, *Philosophical Transactions of the Royal Society of London A: Mathematical, Physical and Engineering Sciences*, *375*(2102), doi:10.1098/rsta.2016.0325.

Parekh, P., F. Joos, and S. A. Müller (2008), A modeling assessment of the interplay between aeolian iron fluxes and iron-binding ligands in controlling carbon dioxide fluctuations during Antarctic warm events, *Paleoceanography*, *23*, PA4202, doi:10.1029/2007PA001531.

Pfister, P. L., and T. F. Stocker (2016), Earth system commitments due to delayed mitigation, *Environmental Research Letters*, *11*(1), 014,010.

Plattner, G.-K., F. Joos, T. F. Stocker, and O. Marchal (2001), Feedback mechanisms and sensitivities of ocean carbon uptake under global warming, *Tellus B*, *53*(5), 564–592, doi:10.1034/j.1600-0889.2001.530504.x.

Plattner, G.-K., R. Knutti, F. Joos, T. F. Stocker, W. von Bloh, V. Brovkin, D. Cameron, E. Driesschaert, S. Dutkiewicz, M. Eby, N. R. Edwards, T. Fichefet, J. C. Hargreaves, C. D. Jones, M. F. Loutre, H. D. Matthews, a. Mouchet, S. a. Müller, S. Nawrath, a. Price, a. Sokolov, K. M. Strassmann, and a. J. Weaver (2008), Long-Term Climate Commitments Projected with Climate–Carbon Cycle Models, *Journal of Climate*, *21*(12), 2721–2751, doi:10.1175/2007JCLI1905.1.

Pörtner, H.-O. (2010), Oxygen- and capacity-limitation of thermal tolerance: a matrix for integrating climate-related stressor effects in marine ecosystems, *Journal of Experimental Biology*, *213*(6), 881–893, doi:10.1242/jeb.037523.

Praetorius, S. K., A. C. Mix, M. H. Walczak, M. D. Wolhowe, J. A. Addison, and F. G. Prahl (2015), North Pacific deglacial hypoxic events linked to abrupt ocean warming, *Nature*, *527*(7578), 362–366.

Randerson, J. T., K. Lindsay, E. Munoz, W. Fu, J. K. Moore, F. M. Hoffman, N. M. Mahowald, and S. C. Doney (2015), Multi-century changes in ocean and land contributions to the climate-carbon feedback, *Global Biogeochemical Cycles*, *29*(6), 744–759, doi:10.1002/2014GB005079, 2014GB005079.

Ridgwell, A., and D. N. Schmidt (2010), Past constraints on the vulnerability of marine calcifiers to massive carbon dioxide release, *Nature Geosci*, *3*(3), 196–200, doi:10.1038/ngeo755, 10.1038/ngeo755.

Ritz, S. P., T. F. Stocker, and F. Joos (2011), A coupled dynamical ocean-energy balance atmosphere model for paleoclimate studies, *J. Climate*, *24*(2), 349–375, doi:10.1175/2010JCLI3351.1.

Roth, R., S. P. Ritz, and F. Joos (2014), Burial-nutrient feedbacks amplify the sensitivity of carbon dioxide to changes in organic matter remineralisation, *Earth System Dynamics*, *5*(1), 321–343, doi:10.5194/esdd-5-473-2014.

Rugenstein, M. A. A., J. Sedláček, and R. Knutti (2016), Nonlinearities in patterns of long-term ocean warming, *Geophysical Research Letters*, *43*(7), 3380–3388, doi:10.1002/2016GL068041, 2016GL068041.

Sanderson, B. M., B. C. O'Neill, and C. Tebaldi (2016), What would it take to achieve the Paris temperature targets?, *Geophysical Research Letters*, *43*(13), 7133–7142, doi:10.1002/2016GL069563, 2016GL069563.

Schmidtko, S., L. Stramma, and M. Visbeck (2017), Decline in global oceanic oxygen content during the past five decades, *Nature*, *542*(7641), 335–339, doi:10.1038/nature21399.

Schmittner, A., A. Oschlies, H. D. Matthews, and E. D. Galbraith (2008), Future changes in climate, ocean circulation, ecosystems, and biogeochemical cycling simulated for a business-as-usual CO2 emission scenario until year 4000 AD, *Global Biogeochem. Cy.*, *22*(1), GB1013—, doi:10.1029/2007GB002953.

Shaffer, G., S. M. Olsen, and J. O. P. Pedersen (2009), Long-term ocean oxygen depletion in response to carbon dioxide emissions from fossil fuels, *Nature Geosci*, *2*(2), 105–109, doi:10.1038/ngeo420, 10.1038/ngeo420.

Shakun, J. D., P. U. Clark, F. He, S. A. Marcott, A. C. Mix, Z. Liu, B. Otto-Bliesner, A. Schmittner, and E. Bard (2012), Global warming preceded by increasing carbon dioxide concentrations during the last deglaciation, *Nature*, *484*(7392), 49–54, doi:10.1038/nature10915.

Steinacher, M., and F. Joos (2016), Transient Earth system responses to cumulative carbon dioxide emissions: linearities, uncertainties, and probabilities in an observation-constrained model ensemble, *Biogeosciences*, *13*(4), 1071–1103, doi:10.5194/bg-13-1071-2016.

Steinacher, M., F. Joos, L. Bopp, P. Cadule, S. C. Doney, M. Gehlen, B. Schneider, and J. Segschneider (2009), Projected 21st century decrease in marine productivity : a multi-model analysis, *Biogeosciences*, pp. 7933–7981.

Steinacher, M., F. Joos, and T. F. Stocker (2013), Allowable carbon emissions lowered by multiple climate targets, *Nature*, *499*, 197–201, doi:10.1038/nature12269.

Storch, D., L. Menzel, S. Frickenhaus, and H. O. Pörtner (2014), Climate sensitivity across marine domains of life: limits to evolutionary adaptation shape species interactions, *Global Change Biology*, *20*(10), 3059–3067.

Sweetman, A. K., A. Thurber, C. Smith, L. Levin, C. Mora, and C. L. Wei (2017), Major impacts of climate change on deep-sea benthic ecosystems, *Elem Sci Anth*, *5:4*.

Taucher, J., L. T. Bach, U. Riebesell, and A. Oschlies (2014), The viscosity effect on marine particle flux: A climate relevant feedback mechanism, *Global Biogeochemical Cycles*, *28*(4), 415–422, 2013GB004728.

Tschumi, T., F. Joos, and P. Parekh (2008), How important are Southern Hemisphere wind changes for low glacial carbon dioxide? A model study, *Paleoceanography*, *23*, PA4208, doi:10.1029/2008PA001592.

Tschumi, T., F. Joos, M. Gehlen, and C. Heinze (2011), Deep ocean ventilation, carbon isotopes, marine sedimentation and the deglacial CO2 rise, *Clim. Past*, *7*(3), 771–800, doi:10.5194/cp-7-771-2011.

UNFCCC (accessed 11. October 2017), United Nations Framework Convention on Climate Change, Adoption of The Paris Agreement, http://unfccc.int/paris_agreement/items/9485.php.

UNFCCC (accessed 6. February 2018), United Nations Framework Convention on Climate Change, https://unfccc.int/resource/docs/convkp/conveng.pdf.

Weaver, A. J., J. Sedláček, M. Eby, K. Alexander, E. Crespin, T. Fichefet, G. Philippon-Berthier, F. Joos, M. Kawamiya, K. Matsumoto, M. Steinacher, K. Tachiiri, K. Tokos, M. Yoshimori, and K. Zickfeld (2012), Stability of the Atlantic meridional overturning circulation: A model intercomparison, *Geophysical Research Letters*, *39*(20).

Weiss, R. (1974), Carbon dioxide in water and seawater: The solubility of a non-ideal gas, *Mar. Chem.*, *2*, 203–215.

Winkelmann, R., A. Levermann, A. Ridgwell, and K. Caldeira (2015), Combustion of available fossil fuel resources sufficient to eliminate the Antarctic Ice Sheet, *Science Advances*, *1*(8), doi:10.1126/sciadv.1500589.

Yamamoto, A., A. Abe-Ouchi, M. Shigemitsu, A. Oka, K. Takahashi, R. Ohgaito, and Y. Yamanaka (2015), Global deep ocean oxygenation by enhanced ventilation in the Southern Ocean under long-term global warming, *Global Biogeochemical Cycles*, *29*(10), 1801–1815, doi:10.1002/2015GB005181, 2015GB005181.

Zickfeld, K., M. Eby, A. J. Weaver, K. Alexander, E. Crespin, N. R. Edwards, A. V. Eliseev, G. Feulner, T. Fichefet, C. E. Forest, P. Friedlingstein, H. Goosse, P. B. Holden, F. Joos, M. Kawamiya, D. Kicklighter, H. Kienert, K. Matsumoto, I. I. Mokhov, E. Monier, S. M. Olsen, J. O. P. Pedersen, M. Perrette, G. Philippon-Berthier, A. Ridgwell, A. Schlosser, T. S. V. Deimling, G. Shaffer, A. Sokolov, R. Spahni, M. Steinacher, K. Tachiiri, K. S. Tokos, M. Yoshimori, N. Zeng, and F. Zhao (2013), Long-Term Climate Change Commitment and Reversibility: An EMIC Intercomparison, *Journal of Climate*, *26*(16), 5782–5809, doi:10.1175/JCLI-D-12-00584.1.

Zickfeld, K., S. Solomon, and D. M. Gilford (2017), Centuries of thermal sea-level rise due to anthropogenic emissions of short-lived greenhouse gases, *Proceedings of the National Academy of Sciences*, *114*(4), 657–662.